ACS Catalysis

pubs.acs.org/acscatalysis Research Article

Exchange Current Density as an Effective Descriptor of Poisoning of Active Sites in Platinum Group Metal-free Electrocatalysts for Oxygen Reduction Reaction

Valerio C. A. Ficca, Carlo Santoro,* Ernesto Placidi, Fabrizio Arciprete, Alexey Serov, Plamen Atanassov, and Barbara Mecheri*

Cite This: *ACS Catal.* 2023, 13, 2162−2175 Read Online

ACCESS | Metrics & More | Article Recommendations | Supporting Information

ABSTRACT: The oxygen reduction reaction (ORR) is of primary importance for the direct and clean conversion of energy in fuel cells, necessarily requiring an electrocatalyst to be exploited. At the state of the art, platinum group metal-free (PGM-free) electrocatalysts are the most promising alternative to carbon-supported Pt nanoparticles (Pt/C), which are more expensive and more performing but highly prone to deactivation in a contaminated working environment. The comparison of the two materials is at the level of fine-tuning, requiring specific activity descriptors, namely, turnover frequency (TOF) and site density (SD), to understand how to compare the performance of PGM-free electrocatalysts with Pt/C electrocatalysts. Specific probing molecules that bind with the active sites are required to evaluate the SD of PGM-free electrocatalysts. However, PGM-free electrocatalysts possess not a single active site like Pt/C, but a multitude of primary (metal-containing) and secondary (metal-free) sites arising from the pyrolysis synthesis process, eventually complicating SD evaluation. In this work, we propose a method for evaluating the direct interaction through the chemisorption of probing molecules over the PGM-free primary and secondary sites, the discrimination of which is of paramount importance in an effective SD evaluation. Based on the rotating disk electrode technique, the study investigates the electrochemistry of Fe-based PGM-free electrocatalysts poisoned with hydrogen sulfide at pH 1 in comparison with a Pt/C sample. In addition, X-ray photoelectron spectroscopy (XPS) is used to establish a relationship between the electrochemistry and surface chemistry of the poisoned material. The results identify the exchange current density as a meaningful tool that allows the discrimination of poisoning of specific active sites (metal-containing or metal-free). In addition, the understanding of the interaction phenomenon occurring between sites and probing molecules will be paramount for the selection of those contaminants capable of selectively interacting with the active sites of interest, paving the way to a more accurate SD evaluation.

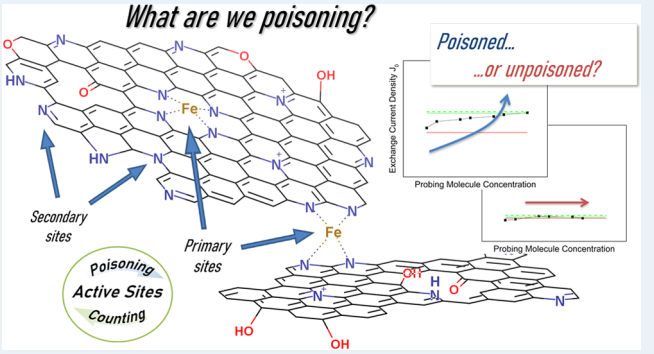

KEYWORDS: *PGM-free electrocatalysts, Pt/C electrocatalysts, active sites, poisoning, Tafel slope, Koutecky−Levich analysis, activity descriptors, exchange current density*

1. INTRODUCTION

Platinum group metal-free (PGM-free) electrocatalysts are the most promising alternatives for platinum substitution in energy conversion devices such as low-temperature fuel cells (FC) and metal−air batteries.[1] Nowadays, FC technology based on hydrogen is emerging not only as a promising alternative for reducing fossil fuel consumption and, consequently, greenhouse gases (GHG) but also because Li-battery technology will not suffice to completely replace internal combustion engines.[2] This is mainly due to problems related to strategic elements like Li and Co, manufacturing costs, and affordability. In addition, net surplus electricity already produced from renewable sources could be usefully exploited in electrolyzers to increase the production of green hydrogen[3] and boost FC application.

However, the oxygen reduction reaction (ORR) at the cathode side of FC requires specifically designed electrocatalysts due to their sluggish kinetics and multiple steps compared to faster hydrogen oxidation.[4,5] At the state of the art, platinum group metals (PGMs) are the reference materials

Received: October 22, 2022
Revised: December 17, 2022

for the ORR; Pt is the most performing electrocatalyst for the acidic environment while Pd is the alkaline counterpart,[6−9] but both elements hold the crucial issues of economic affordability and stability upon contamination. Nevertheless, the need for affordable, scalable, sustainable, and durable electrocatalysts is the driving force in replacing Pd- and Pt-based electrocatalysts.

Currently, two reactivity descriptors are exploited for comparing the electrocatalytic activity of PGM and PGM-free electrocatalysts: the turnover frequency (TOF, *i.e.*, the number of electrons transferred per second per active site at a specific potential) and the number of sites per square centimeter (or per gram) of electrocatalyst (SD, *i.e.*, site density).[10−12] Typical values of TOF for Pt and PGM-free electrocatalysts are, respectively, 10−42 e^- $site^{-1}$ s^{-1} and below 2 e^- $site^{-1}$ s^{-1}.[10,12−14] Regarding SD, Pt and PGM-free electrocatalysts possess a (gravimetric) SD, respectively, in the order of $\sim 10^{20}$ and $\sim 10^{19}$ sites g^{-1}.[12] The lower SD in PGM-free electrocatalysts was calculated to correspond to one site every ∼70 nm.[15] In comparison, two adjacent Pt atoms are 2.6−2.8 Å apart,[16,17] while the bond length of gas-phase O_2 is 1.225 Å.[18]

In carbon-supported Pt nanoparticle electrocatalysts (Pt/C), the catalytic sites are hosted on structural units of 2−5 nm in diameter,[19] having a crystal structure and hundreds of surface atoms.[20,21] Conversely, the active sites of PGM-free electrocatalysts are inspired by nature to hemoglobin: they are composed of a single transition metal atom center coordinated with multiple nitrogen atoms (M−N_x−C coordination, x = 1−4, M = Fe, Co, Mn, Sn).[11,12,22−26] Usually, iron is largely exploited for the ORR in its most active form of Fe−N_x sites, with Fe(II) in the role of an oxygen binder. In PGM-free electrocatalysts, the C matrix containing the M−N_x sites is the material backbone and is usually interconnected with heteroatoms like N, S, B, and P in percentages between 1 and 10 wt %.[27]

When acting as an electrocatalyst, Pt/C behaves like a two-component material, with metallic nanoparticles being active at higher potentials (between 1.0 and 0.7 V vs reversible hydrogen electrode (RHE)) and with C support being active at potentials lower than 0.65 V vs RHE.[28] Considering FC operation voltages around 0.9 V vs RHE, the ORR on Pt does not suffer additional overpotential arising from the support but just contributions ascribable to Pt surface activation.[29−31] Conversely, a PGM-free electrocatalyst is a whole single material, with Fe−N_x as primary sites and N functionalities in the C matrix (pyridinic and pyrrolic (or protonated) N, graphitic, and quaternary N) as secondary active sites (referred to as NC), both showing an ORR activity.[22,32−34] The onset of the ORR in Fe−N_x electrocatalysts is related to the availability of Fe^{2+}−N_x centers originating from Fe^{3+}/Fe^{2+} redox transition, corresponding to the potential required for the transition from Fe^{3+} (oxide-covered metal) to Fe^{2+} (oxide-free metal).[35,36] In addition, the electronic properties of the C basal plane influence the Fe^{3+}/Fe^{2+} redox transition potential. Disrupting the π-electron delocalization of the basal plane resulted in shifting the Fe^{3+}/Fe^{2+} couple toward more positive potentials.[1,35,37] Similar effects are obtained with the reduction of the lateral size of C sp^2 planes[1,38,39] or the introduction of sulfur functionalities possessing electron-withdrawing ability (C−SO_x).[38,40,41] However, the decrease in lateral size corresponds to a higher degree of plane edges, which are more prone to oxidation.[42] The whole material is thus catalytically active in the same potential interval as Pt/C, with the C matrix impacting the reactivity of active sites, leading to additional drawbacks on the ORR in terms of efficiency losses.[43]

On Pt/C electrocatalysts, the ORR follows two parallel routes: a predominant four-electron (4e^-) reaction to water and a side 2e^- reaction to peroxide.[4] The amount of peroxide depends on strongly adsorbed species and the ionomer binder used to produce the ink.[28] Similarly, the ORR on PGM-free electrocatalysts can follow the same paths with a higher contribution of the 2e^- route, ascribable to lower binding energies of the intermediates with respect to Pt.[4] Moreover, differently than Pt, PGM-free electrocatalysts can also catalyze a 2 × 2e^- pathway, characterized by the production of the intermediate and the subsequent reduction to water on the same site or adjacent close sites.[44] The active sites for the different paths have also been identified.[44] Fe−N_x are considered sites for the 4e^- or 2 × 2e^- paths, while metal-free sites can produce either peroxide (pyrrolic, graphitic, quaternary, or N-protonated) or convert peroxide to water (pyridinic N).

The reaction mechanism and the rate-determining step (RDS) are still debated despite the knowledge of the number of electrons involved. The reaction certainly involves three adsorbed intermediates: atomic oxygen (O_{ads}), hydroxyl (OH_{ads}), and superoxide (OOH_{ads}),[21,45−47] generated from three elementary steps (with or without proton involvement), O_2 bond breaking, O reduction, and OH reduction.[48] Nevertheless, the uncertainty on the reaction mechanism is additionally complicated by external parameters such as the nature of the electrocatalyst, the oxide coverage, the applied potential, the solvent's nature, and the working temperature.[21,48−51]

Among the additional factors, the oxide coverage is the one most impacting the overpotential. On Pt held at high potentials, the oxide layer is caused by water activation in acidic aqueous solutions, whereas it is ascribable to hydroxyl-specific adsorption in alkaline media.[4,29−31,52] Due to the different oxide coverage in acidic media, the reaction proceeds with the activation of the surface and the subsequent chemisorption of molecular oxygen in a surface-dependent ORR localized at the inner Helmholtz plane (IHP). In the IHP, inner-sphere electron transfer (ET) reactions occur, mediated by surface adsorbed (and stabilized) intermediates, following thus a 4e^- path. In alkaline media, the OH-blocked surface promotes the ORR of solvated oxygen in the outer Helmholtz plane (OHP). In the OHP, the ORR evolves with a surface-independent outer-sphere ET, which is nonspecific on the nature of the catalytic material, resulting in a 2e^- path.[4] However, in Pt/C, both inner-sphere and outer-sphere ET coexist at alkaline pH, leading to the 4e^- path.[4] Similar to Pt, the ORR on PGM-free electrocatalysts is also affected by pH, with a mechanism depending on the metal and the presence of secondary phases. Among the different metals, iron is more active than cobalt[25,53] since the peroxide reduction is shifted anodically (more positive) with respect to the ORR, thus favoring its immediate reduction to water.[5] For single Fe atoms (Fe−N_x), the ORR mechanism involves an inner-sphere ET at acidic pH. However, above a certain pH (>10.5), the mechanism changes toward the outer sphere[54,55] and, at pH 13, is believed to evolve with a mixed ET.[1] Indeed, above pH 10.5, the single Fe atom sites are oxide-free,[56] promoting an inner-sphere ET; by contrast, the support is oxide-covered, possessing the typical outer-sphere ET with the 2e^-

https://doi.org/10.1021/acscatal.2c05222
ACS Catal. 2023, 13, 2162−2175

mechanism. At pH ≥ 14, a $2e^-$ process is the only one occurring for all of the electrocatalysts, except for Ru-based materials.[5,22] To visualize the two ORR pathways of PGM-free electrocatalysts, a schematization is reported in Table S1.

The higher activity of Pt/C structural units corresponds to a behavior extremely sensible to the working environment, prone to deactivation if operated in a contaminated environment.[57−62] In pyrolyzed PGM-free electrocatalysts, stability issues in the acidic medium are ascribable to the $2e^-$ path, with demetallation of active sites and C support corrosion upon interaction with H_2O_2 via Fenton reactions.[63,64] Nevertheless, Fe−N_x−C has a higher tolerance to contaminated working environments with respect to Pt.[36,65,66] This is mainly due to the lower interaction between the Fe active site and the ion of interest. Indeed, Pt-based electrocatalysts are poisoned by many different byproduct molecules found in reaction precursors (especially those from fossil fuels), with amounts as low as ppm.[67−72] In the case of sulfur contamination, an amount of sub-ppm or ppb is already sufficient to severely affect the catalytic activity of Pt electrocatalysts.[73,74] The predominant origin of contamination of Pt-based materials is the competitive chemisorption of unwanted molecules, blocking or reducing the adsorption of reacting molecules, hence inhibiting electrocatalysis. A minor contribution also arises from reduced membrane/ionomer conductivity impacting the device performance.[75,76]

Typical contaminant molecules of Pt surfaces are sulfur dioxides (SO_2),[77−79] elemental S,[70] hydrogen sulfide (H_2S),[68,73] carbonyl sulfide (COS),[61,80] ammonia (NH_3), ammonium ion (NH_4^+),[75,76,81] phosphate ($H_2PO_4^-$ at pH 1),[82] nitrogen oxides (NO_x),[83,84] carbon monoxide (CO),[71,85] halide ions,[86−89] and methanol.[90] Many of these contaminants are present as impurities in the anodic fuel used for FC (CO, CO_2, H_2S, and NH_3), while others as air pollutants of the cathode side (NO_x, SO_x, CO, and CO_2).[67,68,72−74,91,92] Among the contaminants, S-containing molecules are the most impacting on performance due to strong adsorption bonds. Nevertheless, using appropriate protocols for FC operations, it is possible to recover the catalytic activity polarizing at high potentials to oxidize the adsorbed S to sulfates that are then desorbed from the catalytic site.[68,73,92] The problem of sulfur contamination of Pt catalysts is a well-known issue. The amount of H_2S and S species in contact with the Pt surface must be kept tremendously low (<10 ppb) to maintain the catalytic performance.[93] Indeed, a single S atom can deactivate catalytic surface planes upon crystallographic plane reorganization induced by fast surface diffusion processes.[62] The contamination is thus the result of a reorganization of the surface planes driven by the reduction in the surface free energy, evolving into a new plane orientation with adsorbed S atoms. In addition, the strong bond between Pt and S can introduce electronic perturbations in the metal, with a reduction in the density of states of the 5d band near the Fermi level, subsequent to the charge transfer from the metal to the S atoms.[60] The result is a change in the ORR from the $4e^-$ to the $2e^-$ pathway with peroxide production.[94]

Regarding PGM-free electrocatalysts, many anions were tested as possible contaminants in the last decade, mainly focusing on the Fe-coordinated sites. Nowadays, the quantification of the SD is performed with molecular probes capable of interacting with the active sites. These were first used to corroborate the identification of the active sites (Fe−N_x) and later to compare the ORR activity quantitatively and qualitatively with respect to Pt/C, especially in FC applications. However, the absence of a standardized protocol led to different (and often contradictory) results, considering that the site identifications were performed in acid, neutral, and alkaline environments. Nevertheless, it is worthwhile mentioning that the poisoning of PGM-free electrocatalysts never results in a total deactivation of electrocatalysis but just a decrease in performance. This is very different compared to Pt/C, which can be completely deactivated (*e.g.*, S contamination). To date, no attempts to identify markers for the poisoning were investigated, except in one case.[95] Only a few studies were centered on the mechanism of ORR poisoning with the aim of developing a protocol for SD identification in PGM-free electrocatalysts: Malko et al. studied nitrite poisoning and stripping at pH 5.2 using an acetate buffer;[96] Chakraborty et al. indirectly evaluated SD in metal-free NC electrocatalysts using catechol operating in phosphate buffer (pH 7);[32] Bae et al. studied the irreversible cyanide contamination for spectrophotometric quantification of SD at pH 1, 7, and 13;[97] Boldrin et al. studied the NO adsorption for a protocol of super-activation of PGM-free electrocatalysts at pH 1 and 7.[43] However, the methods based on probing molecules have drawbacks related to the nature of the molecule itself. Gaseous molecules tend to overestimate the SD accessing micropores that are commonly flooded during FC operation, interacting with other structural units like nanoparticles, and also adsorbing with non-Langmuir models (layered adsorption). Differently, the molecules used in the electrolyte solutions tend to underestimate the SD due to difficulties in accessing the deepest pores. Overall, all of them do not have a control system to check which site they are interacting with.

Overall, pyrolyzed PGM-free electrocatalysts are known to be unaffected by the presence of methanol, chloride, urea, benzene, toluene, NH_4^+, CO, SO_2, S^{2-}, and SO_4^{2-} in FC applications in a broad range of pH[36,66,98−102] and nitrate (NO_3^-), perchlorate (ClO_4^-), fluoride (F^-), ethanethiol (EtSH), and sodium azide (NaN_3) in half-cell tests.[95,103] In metal-free NC electrocatalysts, CO and CN^- tests resulted in no interaction, while upon H_2S treatment at 350 °C, NC was positively affected by sulfur co-doping.[104,105] Conversely, a dihydrogen phosphate ion ($H_2PO_4^-$, pH 1) and 1,2-dihydroxybenzene (catechol, pH 7) were found to interact.[32,106] Regarding Fe−N_x, various anions and compounds can interact with the active sites decreasing the ORR activity, such as cyanide (CN^-, pH 1 and 13), thiocyanate (SCN^-, pH 1 and 13), hydrogen sulfide (H_2S, pH 1), nitrite (NO_2^- acidic and neutral), hydroxylamine (NH_4OH, pH 7), and tris(hydroxymethyl)aminomethane (Tris, pH 1 and 13).[38,56,96−98,103,107−116] At the same time, gaseous molecules like nitrogen monoxide (NO) were also used as molecular probes.[43,114]

Previously, we reported a study on developing a protocol for identifying the fingerprint of Fe−N_x catalytic site contamination based on the investigation of PGM-free electrocatalyst poisoning with nitrite and other contaminants in neutral media.[95] We have now extended our research, reporting a new poisoning study devoted to identifying a suitable marker for discriminating the contamination of metal-containing and metal-free active sites. Exploiting as a control the effect of sulfur-containing compounds on Pt, able to completely deactivate its catalytic activity, their effect on PGM-free electrocatalysts is investigated in detail through parallel

https://doi.org/10.1021/acscatal.2c05222
ACS Catal. 2023, 13, 2162−2175

electrochemical and spectroscopic approaches. Compared to the reference case of nitrite, where the contamination occurred selectively over the Fe−N_x coordination, the results obtained with hydrogen sulfide were useful for identifying the exchange current density (J_0) as a suitable marker for the identification of the poisoning of metal-containing and metal-free active sites. The finding will be crucial for developing more appropriate protocols for SD identification, allowing to discriminate among contaminants capable of selecting specific active sites.

2. MATERIALS AND METHODS

2.1. Catalyst Preparation. The Fe−N−C electrocatalyst derived from benzimidazole (BZIM) and named as FeBZIM was synthesized as previously reported.[117] Briefly, FeBZIM was obtained through the sacrificial support method (SSM) using low surface area monodispersed silica (OX50, 45 $m^2\ g^{-1}$) as a template, benzimidazole (BZIM) as a nitrogen and carbon precursor, and iron nitrate as a metal-containing precursor. The three compounds were mixed and pyrolyzed at 900 °C under a controlled atmosphere (UHP nitrogen, 100 $cm^3\ min^{-1}$) for 45 min. The resulting powder was then washed in 24 wt % hydrofluoric acid for 48 h to remove the inorganic compounds like silica, carbides, carbo-nitrides, metallic iron, and oxides. The final product was washed repeatedly until a neutral pH was achieved, hence dried overnight at 80 °C. After this step, a 20 min 450 rpm ball milling treatment was performed, obtaining a finely dispersed powder material labeled FeBZIM.

2.2. Ink Preparation. The electrocatalyst inks were prepared by dispersing either 4 mg mL^{-1} of FeBZIM or 1 mg mL^{-1} of platinum (Pt nominally 40 wt % on carbon black, HiSPEC 4000, Alfa Aesar) (Pt40CB) catalyst in 637 μL of deionized (Millipore) water (DI, 18.2 MΩ cm@25 °C), 213 μL of isopropyl alcohol (IPA) (HiPerSolv Chromanorm, VWR Chemicals), and 150 μL of diluted Nafion 0.5 wt % (Nafion 5 wt % in lower aliphatic alcohols and water, Aldrich). The suspension was ultrasonicated for 30 min at a temperature of 15 °C for FeBZIM and 5 °C for Pt40CB. The catalyst layer was prepared by drop-casting an aliquot of the ink onto the glassy carbon electrode to achieve a final loading of 0.2 mg cm^{-2} (FeBZIM) or 0.04 mg cm^{-2} (Pt40CB). The electrode with the drop-casted solution was then placed over a heating plate at 50 °C and left to completely dry under a glass bell containing a humidified atmosphere from bubbling nitrogen into a solution of IPA:DI 17:3 v/v.

2.3. Electrochemical Tests. The tests were performed using a rotating disk electrode (RDE) technique operated in linear sweep voltammetry (LSV) and controlled by VMP3 Potentiostat (Bio-Logic Science Instruments) using EC-Lab software. The setup consisted of a conventional three-electrode cell with a saturated calomel electrode (SCE) (Amel 303/SCG/12) as the reference electrode, a graphite rod as the counter electrode, and glassy carbon (Pine AFE3T050GC) with the catalyst layer as the working electrode.

All glassware was cleaned in a piranha solution (3:1 v/v mixture of 96% H_2SO_4 and 30% H_2O_2), followed by at least seven boiling steps with DI to remove any residual sulfates and other contaminants.

The study was performed at controlled room temperature (25 °C), exploiting three different electrolyte solutions: 0.1 M perchloric acid ($HClO_4$, pH 1), 0.1 M phosphate buffer solution (PBS, pH 7), and 0.1 M potassium hydroxide solution (KOH, pH 13). All of the potentials were recorded vs SCE and converted to RHE. Before measurements, the electrolyte solution was purged with nitrogen for 20 min. The catalyst layer was conditioned using cyclic voltammetry (CV) between 1.2 and 0 V vs RHE at 50 mV s^{-1} for three cycles and then CV at 500 mV s^{-1} until voltammograms became stable with cycles. After that, the solutions were purged with oxygen for 20 min, and then the LSV scans were performed at an electrode rotation rate of 1600 rpm and a potential scan rate of 5 mV s^{-1} between 1.0 and 0.1 V vs RHE four times. These pristine scans were labeled with the name of each electrolyte solution ($HClO_4$, PBS, and KOH). From the collected data, three main parameters of interest were extrapolated: onset potential (E_{onset}) obtained at −0.1 mA cm^{-2}, half-wave potential ($E_{1/2}$), and limiting current density (J_{lim}) at a potential of 0.20 V vs RHE. These parameters were used as indicators of catalytic activity, and their trends were observed throughout the poisoning tests. All of the data reported herein were background-subtracted and *iR*-corrected.

2.4. Poisoning Tests. Two different sulfur-containing contaminants were used for this study: sulfate (SO_4^{2-}) and sulfide (S^{2-}) anions, added stepwise increasing concentrations of 0.05, 0.1, 0.5, 1, 5, 10, and 50 mM in the form of sodium salts (Sigma-Aldrich). The solution pH was checked to be constant after each addition of the salts.

The electrocatalyst poisoning was performed outside the test cell, dipping the RDE electrode modified with the catalytic layer in the electrolyte solution containing the contaminant at the lowest concentration (0.05 mM), followed by spinning the electrode at 300 rpm for 3 min and by a further 1-min deionized water (DI) dipping at 300 rpm to clean the electrode and avoid test cell contamination. In the meanwhile, the electrochemical cell containing either $HClO_4$ (pH = 1), PBS (pH = 7), or KOH (pH = 13) was purged with oxygen. After that, the poisoned RDE is tested again to acquire four LSV scans at 5 mV s^{-1}. Hence, the concentration of the contaminant solution was increased stepwise, and the poisoning procedure was repeated up to 50 mM. Each contaminant step was labeled as the concentration of the contaminant (0.05, 0.1, 0.5 mM, etc.). After the last step of 50 mM, the electrode was washed to check for the electrocatalyst recovery, spinning the RDE in DI at 1600 rpm for 10 min. At the same time, the electrolyte solution was replaced with a fresh 20-min-oxygen-purged solution, and the ORR activity was tested with LSV scans, labeling these scans as "WASH". In the case of no system recovery, a stripping procedure was applied to perform a CV at 100 mV s^{-1} between 1.2 and 0 V vs RHE for 100 cycles.

2.5. Koutecky−Levich (KL) and Tafel Plots. The number of electrons exchanged (n) during the ORR was evaluated by acquiring the Koutecky−Levich (KL) plots from LSV at different electrode rotation rates (ω): 400, 800, 1200, 1600, and 2000 rpm. KL plots were obtained by plotting the reciprocal current density versus the reciprocal square root of the rotation rate, following the KL equation

$$\frac{1}{J} = \frac{1}{J_k} + \frac{1}{J_D} \tag{1}$$

$$J_D = 0.620nFD^{2/3}\upsilon^{-1/6}C\omega^{1/2} \tag{2}$$

where J_k is the kinetic current density, J_D is the limiting current density, n is the number of transferred electrons per mole, F is the Faraday constant (96 485 C mol^{-1}), D is the diffusion

https://doi.org/10.1021/acscatal.2c05222
ACS Catal. 2023, 13, 2162−2175

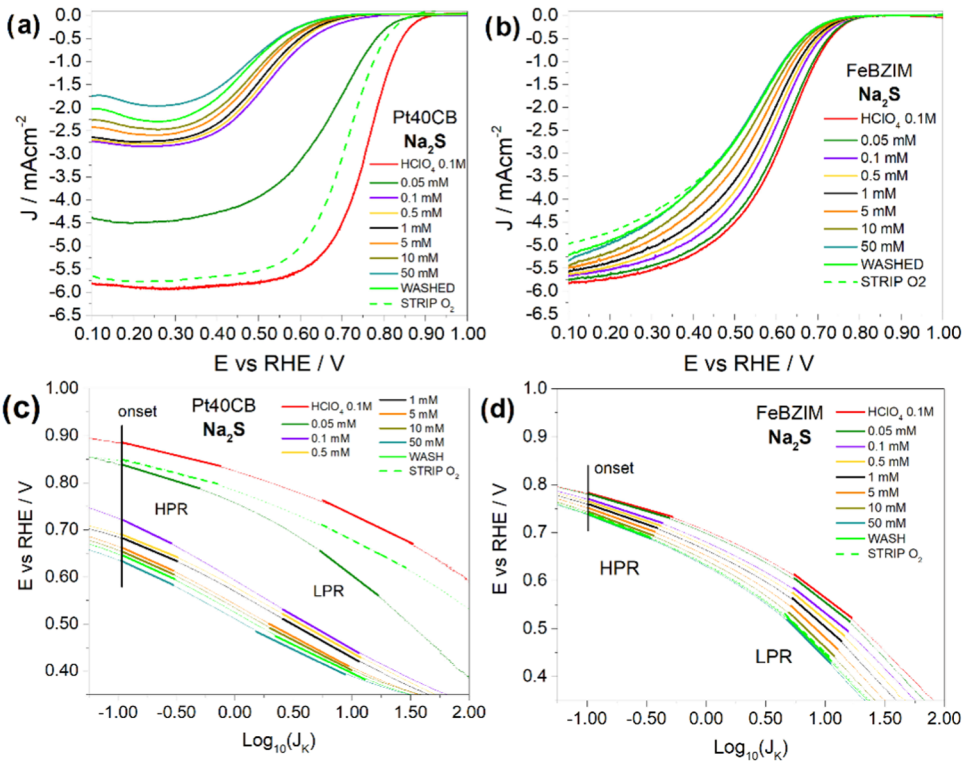

Figure 1. LSV sigmoid at 5 mV s^{-1} and 1600 rpm between 0.10 and 1.00 V vs RHE in 0.1 M $HClO_4$ at the variation of Na_2S concentration from 0.05 mM up to 50 mM for (a) Pt40CB and (b) FeBZIM. Tafel analysis of E vs $\log_{10}(J_k)$ obtained from the previous LSV sigmoid corrected for mass transport, using identical criteria for slope evaluation, for (c) Pt40CB and (d) FeBZIM. Two slopes are identified: a high potential region (HPR) after the onset and a low potential region (LPR) after the half-wave potential and before reaching the mass-transfer-limited region. An uncontaminated electrocatalyst ($HClO_4$ 0.1 M, solid red lines), tests after washing (WASHED, light green lines), and stripping in O_2 (STRIP O_2, dashed light green lines) are also reported.

coefficient (1.93×10^{-5} cm^2 s^{-1}) at pH 1, υ is the kinematic viscosity (0.01 cm^2 s^{-1}), and C is the concentration of oxygen in the electrolyte solution (1.26×10^{-6} mol cm^{-3}) at pH 1. For a complete list of parameters, check Table S2 in the Supporting Information.

The Tafel plots were obtained from the LSV scans at 1600 rpm and 5 mV s^{-1} plotting the potential versus the logarithm of the mass-transport-corrected kinetic current density

$$J_k = \left| \frac{J_D \times J}{(J_D - J)} \right| \tag{3}$$

where J is the current density recorded from the LSV scans and J_D is the value of the mass-transfer-limited current density extrapolated at the point of 0.20 V vs RHE. From the Tafel plots, two different slopes can be fitted: the high potential region (HPR) slope obtained at low current density just after the onset potential for a potential interval of 50 mV, and the low potential region (LPR) slope obtained at high current density, from the half-wave potential over a 90 mV range and before the system enters the mass-transfer-limited region. From HPR/LPR Tafel slopes, the exchange current density (J_0) was evaluated as the point where the y-intercept equals the O_2/H_2O standard potential of 1.229 V vs RHE. Error bars reported for the calculated parameters represent the mean absolute deviation of at least two independent replicates.

2.6. X-ray Photoelectron Spectroscopy (XPS) Analysis. X-ray photoelectron spectroscopy (XPS) was performed using an Omicron DAR 400 Al/Mg Kα non-monochromatized X-ray source and a VG-CLAM2 electron spectrometer. The samples were dispersed in ethanol to a 2 mg mL^{-1} content and deposited onto a 20 nm Au-sputtered n-type silicon wafer (111). The contaminated samples were prepared by dispersing the FeBZIM in a DI water solution containing either 2.5 mM Na_2S or 250 mM Na_2SO_4, ultrasonicated for 30 min, and stirred overnight. The suspension was then vacuum filtered and washed with 50 mL of DI water to remove any remaining salt traces, and the product was then collected and dried for 3 h at 70 °C. The Au 4f spectrum was collected as a reference, while the C 1s, N 1s, O 1s, and S 2p spectra were collected for this study.

3. EXPERIMENTAL DATA AND DISCUSSION

3.1. Electrochemical Analysis. The two classes of electrocatalysts, PGM and PGM-free electrocatalysts, are known to possess high performance in ORR electrocatalysis. The nature of the underlying constituents has been introduced, resulting in characteristic trends when operated in half-cell tests at hydrodynamic conditions. In Figure S1, the linear sweep voltammetry (LSV) at 1600 rpm are reported for both electrocatalysts at the three pH values of interest (1, 7, and 13). The results are discussed in the Supporting Information, giving details about the electrocatalytic performance. It is known from the literature that PGM electrocatalysts have superior activity compared to PGM-free electrocatalysts in acidic pH, predominantly ascribable to stronger adsorption of intermediates over the catalytic surface. Nevertheless, at the increase of hydroxyl concentration, the differences between PGM and PGM-free electrocatalysts are eventually leveled due to the change in the ORR mechanism following the adsorption

https://doi.org/10.1021/acscatal.2c05222
ACS Catal. 2023, 13, 2162−2175

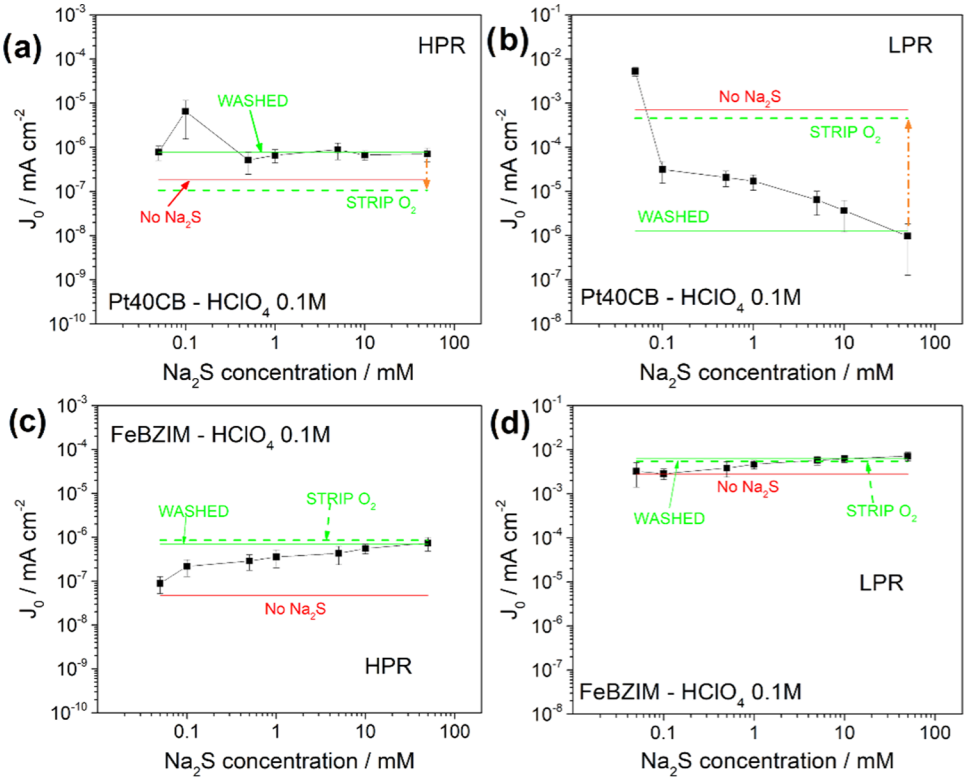

Figure 2. Exchange current density (J_0) of HPR and LPR regions obtained using the protocol mentioned in the Supporting Information, respectively, for Pt40CB (a, b) and FeBZIM (c, d).

of OH^-. From the data reported in Figure S1, it is possible to extrapolate the three main electrochemical parameters: onset potential (E_{onset}), half-wave potential ($E_{1/2}$), and limiting current density (J_{lim}). In addition, upon correcting LSVs for mass transport and applying the Tafel analysis, is it possible to obtain slopes in the unit of mV dec^{-1} from which the exchange current density can be calculated at the thermodynamic potential for the ORR ($E°$ = 1.229 V vs RHE). The detailed protocol for Tafel slope evaluation used in this text is described in the Supporting Information (Determining a Standard Protocol for Tafel Slope Evaluation section), while Table S3 lists a summary of the above-mentioned parameters extrapolated from the LSVs.

3.2. Sulfide and Sulfate Contamination. The effect of S poisoning on Pt has already been studied,[60−62,68,70,73,77−80,92,94] especially in fuel cell applications, reporting different reaction mechanisms.[58] Sulfide and sulfate species are known contaminants of Pt electrocatalysts. Sulfide strongly interacts with Pt surfaces through chemisorption, while sulfate is considered a minor contaminant, mainly acting through strong physisorption. The sulfide poisoning involves S adsorption over the metallic Pt surface and a reorganization of crystallographic planes driven by the reduction in the system's surface free energy.[62] In the case of H_2S contamination, a dissociative mechanism results in the surface adsorption of two S species (S and S oxide) and hydrogen in a linear- or bridge-bonded configuration on one or two atoms, respectively.[58] However, the Pt + S system is susceptible to recovery *via* electrochemical oxidation of adsorbed S upon cycling at different potentials during operation. Nonetheless, the effect of H_2S retains minimum irreversibility due to active site deactivation.[58]

The sulfide poisoning tests in an acidic environment (0.1 M $HClO_4$) for Pt40CB and FeBZIM are reported respectively in Figure 1a,b. At that pH, the S-containing species are only H_2S (Figure S2). Peculiar behaviors observed during the tests on Pt40CB are reported in Note S1, Supporting Information. As the sulfide concentration increased, the poisoning effect on the ORR differed for the two electrocatalysts. In the case of Pt40CB, the impact of the contaminant is evident even at the lowest concentration (see Note S1, Supporting Information), resulting in rapid modification of the sigmoid shape and increased overpotential limitations. Overall, the limiting current density was strongly reduced while E_{on} and $E_{1/2}$ shifted toward less positive values. In the first step (0.05 mM), the drop in performance for Pt40CB was 5.3% (E_{on}), 13.4% ($E_{1/2}$), and 26% (J_{lim}), while for 0.1 mM, the catalytic activity was heavily affected with a loss of 18.4, 31, and 52% in E_{on}, $E_{1/2}$, J_{lim}, respectively. At the maximum concentration (50 mM), the electrocatalyst lost 28, 36, and 68% of its original activity.

By contrast, the poisoning effect on FeBZIM was more gradual than on Pt40CB in the same concentration interval, with a mixed kinetic-diffusion region broadening to the whole potential range, hence shifting the mass-transfer-limited region toward more negative potentials, ascribable to a kinetic bottleneck over the system. A similar trend was already observed in the case of nitrite poisoning at pH 7, forming the nitrosyl adduct over Fe−N_x sites.[95] At the highest contaminant concentration, the catalytic activity only decreased by 5.8% (E_{on}), 15.2% ($E_{1/2}$), and 12.9% (J_{lim}), corresponding to the first contamination step of Pt40CB. For a better comprehension of the poisoning effect on Pt40CB and FeBZIM, the variation trends of the three main electrochemical parameters are reported in Figure S3.

https://doi.org/10.1021/acscatal.2c05222
ACS Catal. 2023, 13, 2162−2175

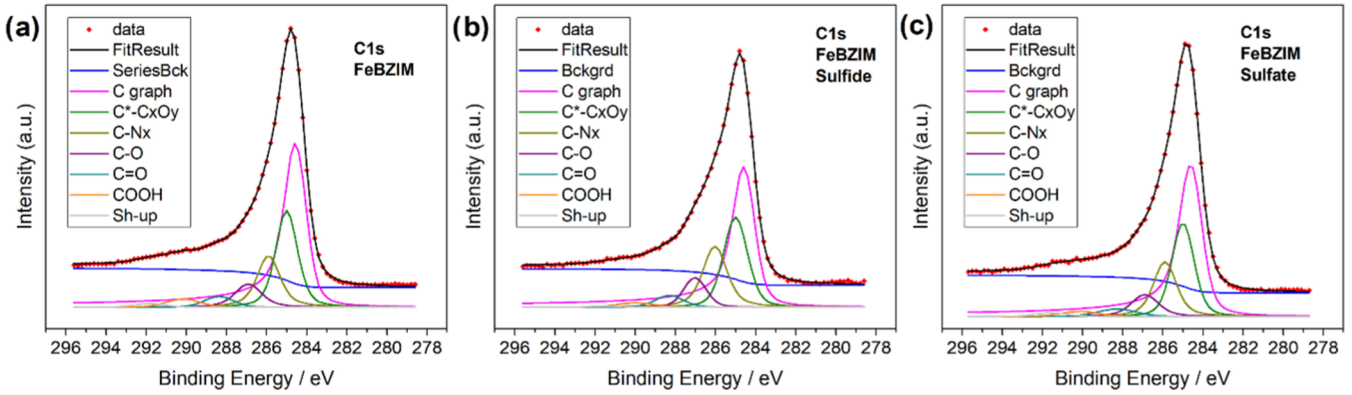

Figure 3. C 1s spectra of pristine FeBZIM (a), FeBZIM contaminated with 2.5 mM of Na_2S (b), and FeBZIM contaminated with 250 mM of Na_2SO_4 (c).

After the last concentration step, the two electrocatalysts underwent a washing and stripping procedure to assess the recovery of the respective systems. Upon washing with DI water at a high rotation speed (1600 rpm), no recovery was observed for both materials, as expected from specifically chemisorbed contaminants. On the contrary, the stripping procedure resulted in an almost complete regeneration of Pt40CB with E_{on}, $E_{1/2}$, and J_{lim}, recovering 98, 94, and 96%, respectively. As reported in the literature, Pt contamination can be reversed by cycling the electrocatalyst to remove the adsorbed sulfur atoms with no specific protocol since plane reorganization is a matter of energy refurbishment.[94,118] Differently, FeBZIM reported no activity recovery after washing and stripping, with a slight further decrease in J_{lim}. This behavior is eventually ascribable to stronger chemisorption energies. However, similar behavior and trends were already observed for nitrite contamination at pH 7,[95] but with partial recovery of the original activity.

Applying the protocol for Tafel slope evaluation mentioned in the previous paragraph, Tafel analysis of Pt40CB and FeBZIM (Figure 1c,d, respectively) was performed, with extrapolated parameters reported in Figures S4 and 2. As the Na_2S concentration increased, the HPR slope of Pt40CB increased rapidly toward 120 mV dec^{-1} in the first two steps (0.05 and 0.1 mM) and then stabilized around 110 mV dec^{-1} (Figure S4a). Regarding the LPR slope, in the first concentration step, the slope increased to 170 mV dec^{-1} and gradually decreased to the original value of 120 mV dec^{-1} (Figure S4b). The exchange current densities of Pt40CB for HPR and LPR slopes (Figure 2a,b) started at 1.8×10^{-7} and 7.2×10^{-4} mA cm^{-2}, respectively, and both varied. The J_0(HPR) increased dropwise by about 1 order of magnitude, while J_0(LPR) decreased abruptly by about 3 orders of magnitude, approaching the value of J_0(HPR).

Regarding FeBZIM, the HPR slope increased stepwise in the whole concentration range, reaching a value of *ca.* 100 mV dec^{-1} at the highest contaminant concentration (Figure S4c), while the LPR slope gradually increased to reach 240 mV dec^{-1} at the same point (Figure S4d). In the case of J_0 for HPR and LPR slopes (Figure 2c,d), the values started respectively at 4.7×10^{-8} and 2.8×10^{-3} mA cm^{-2}, and both increased. Similar to Pt40CB, J_0(HPR) increased by about 1 order of magnitude with a surprising correspondence with the nitrite case at pH 7.[95] In this case, J_0(LPR) slightly increased, unlike Pt40CB and the nitrite contamination. For both materials, the washing procedure did not restore the original values, while the stripping procedure allowed for a complete performance recovery for Pt40CB but was ineffective for FeBZIM.

Regarding the number of transferred electrons (#e^-), using the Koutecky−Levich theory, it was possible to obtain additional data. The variation of the ORR electron number for Pt in the case of sulfur poisoning was already assessed in another paper[94] and will not be considered. For FeBZIM, increasing the contaminant concentration (Figure S5), the number of transferred electrons increased from about three to more than four electrons, which is the most efficient path of the ORR. This result confirms the findings already observed in our previous paper[95] concerning parallel reactions occurring along with the ORR when the metallic centers are contaminated with adducts.

The effect on ORR electrocatalysis of sulfate at pH 1 for both Pt40CB and FeBZIM can be found in Figures S6−S8 of the Supporting Information. However, even at high concentrations, the performances of both electrocatalysts are not affected by chemisorption phenomena. As can be seen from the trends reported, the unspecific adsorption over the active sites is not correlated to the mentioned variations in the electrochemical parameters, especially regarding the sigmoid shape variations associated with the onset and half-wave potential losses that are typical of a kinetic bottleneck. The results of sulfate poisoning at pH 1 are thus meant as a comparison for sulfide poisoning, showing the effect of unspecific phenomena occurring over the active sites and mainly due to the buildup of the contaminant at the increase of concentration.

In addition, sulfate and sulfide contamination at pH 7 and 13 are instead reported in Figures S9 and S10. The S-containing species in the electrolyte solutions are shown again in Figure S2. The contamination in neutral and alkaline environments is of secondary importance due to the nonspecific adsorption of sulfate or the presence of different sulfide-free species that do not affect FeBZIM. The data are reported and meant as a comparison for the sulfide case in both cases, indicative of no contamination.

3.3. Spectroscopic Analysis. The surface chemistry resulting from the contamination of FeBZIM with S-containing ions was further investigated using X-ray photoelectron spectroscopy (XPS). Spectroscopic analysis is meant to bridge the chemistry of the active surface area of the PGM-free electrocatalyst with its electrocatalytic performance reported above, explicitly identifying the adsorbed species. XPS was performed on three different samples: pristine, sulfide-

https://doi.org/10.1021/acscatal.2c05222
ACS Catal. 2023, 13, 2162−2175

poisoned, and sulfate-poisoned FeBZIM, whose C 1s spectra are shown respectively in Figure 3a−c. Additional spectra concerning N 1s and S 2p lines are reported in Figures S11 and S12, Supporting Information, while a summary of elemental composition and chemical speciation is present in Tables S4 and S5. Due to the low iron content (about 0.2%), standard laboratory equipment cannot perform satisfactory Fe 2p spectra to be accurately fitted.

Since PGM-free electrocatalyst synthesis mainly relies on the mechanical mixing and subsequent pyrolysis of precursors in a controlled atmosphere, the resulting material is characterized by various functionalities for both C and N atoms.[22] Different C moieties are identified in the energy range 284−294 eV, particularly graphitic or sp^2 carbon at 284.5 eV, sp^3 carbon (C*/C*x*O*y*) between ∼284.9 and 285.5 eV, and N-bonded carbon ∼285.7−286.4 eV, partially overlapping. In addition, three different oxidized species are also present, C−O, C═O, and COOH, in the range 287−290 eV. A shake-up contribution due to π-conjugation is also found. Regarding nitrogen, seven different functionalities are found in the energy range 396−404 eV: imine (397.6−397.9 eV), pyridinic N (398.5−398.8 eV), Fe-coordinated N atoms (N*x*−Fe, 399.5−399.8 eV), graphitic and pyrrolic or protonated N (Ngr/N−H, 400.6−400.9 eV), graphitic and quaternary N (Ngr/N+, 401.5−402.5 eV), and two N oxides like pyridinic N^+O^- (NO_x, above 403 eV).[44,117,119,120] Finally, S 2p spectra can be fitted using four different contributions in the energy range 160−173 eV. At lower energies, sulfide and pyrite contributions have been identified (S^{2-}/Fe−S_2, 161.5−162.5 eV);[104,121−123] in particular, segregated sulfur on top of oxidized Fe has been identified at 161.7 eV.[123] The identification of chemical speciation in the 163−164 eV interval is more complicated and is usually associated with the carbon bond to sulfur in thiols and disulfides (C−S/C−S−S).[66,113,124−126] Elemental sulfur is identified at 164.1 eV.[124] Above 165 eV, it is possible to find oxidized forms of sulfur, like sulfite (SO_3^{2-}, 165−166 eV).[104,113,121,122] At the highest binding energies, sulfate and iron sulfate contributions are reported (SO_4^{2-}, 168−169 eV).[66,104,121,124]

The presence of residual salts was tested by collecting the Na 1s spectra over contaminated samples: no contributions were present (data not shown); therefore, the S lines are all ascribable to sulfur interacting with the electrocatalyst. The contributions used to fit the spectra of the elements were constrained to have the same linewidth, comprised between 1.1 and 1.2 eV, except for oxide species and shake-up features.

C 1s spectra of the three samples showed the typical asymmetrical main structure of conductive graphitic materials arising from the sp^2-coordinated C═C contribution.[127] The second major contribution is ascribable to sp^3 C bonded to N or O, with a lower contribution of oxides. Upon contamination, FeBZIM with sulfide resulted in a sensible broadening of the full-width half-maximum (FWHM) of C 1s with respect to pristine and sulfate samples (Figure 3b versus 3a,c). The broadening, located in the energy range 284−287 eV, is associated with the increase in the contribution of sp^3 carbon, eventually arising from additional oxidation of the carbon matrix or from S interacting with C. Considering the defective nature of the material, both hypotheses are plausible with preferential sites at the edges of graphitic planes and/or in defects within planes, where dangling bonds increase the excess energy of the system.[104,124] In addition, the shake-up contribution is reduced according to the lower C═C component. However, due to the C−S line (285.7 eV)[123,128] being located between C*/C*x*O*y* and C−N, further discriminating the chemical shifts is not possible. No broadening is reported for sulfate-contaminated FeBZIM (Figure 3c), where components are comparable to pristine FeBZIM, indicating a specific effect of sulfide poisoning.

At the same time, the N 1s spectrum of FeBZIM (Figure S11a) resulted in a significant contribution of protonated and pyridinic nitrogen, followed by N coordinated to iron and graphitic/quaternary species. Minor contributions from oxides (one component) and imine are also present. Sulfur contamination of FeBZIM modified the shape of N 1s, with a sharpening of the spectrum and reduction of the shoulder at 398.5 eV associated with pyridinic N, again upon interaction with sulfide, and the disappearance of the imine contribution (Figure S11b). A general reduction in the oxidation of N is also reported. Minimal or no effects on the same components for the sulfate sample are reported, with an increase in the oxide region (two contributions) (Figure S11b versus S11a,c). Eventually, the interaction of sulfide species with the carbonaceous electrocatalyst also passes through an exchange phenomenon where S replaces pyridinic N, corroborating the hypothesis of S bonding with C. Similar behavior was already reported in the literature where H_2S was employed during the heat treatment of the synthesis process but to a greater extent.[113] The authors also suggested the possibility of sulfur replacing the N species coordinated to Fe, resulting in inhibition of the active sites, but the hypothesis seems not plausible in this context.

Two different configurations of S 2p spectra of sulfur-contaminated FeBZIM are reported (Figure S12). Sulfide-contaminated FeBZIM is in agreement with the literature of both S interacting with Fe and S/N co-doped metal and metal-free PGM-free electrocatalysts.[121−124,129] The analysis showed a predominant contribution associated with S^{2-}/Fe−S_2 at 161.6 eV and a second component arising from sulfates, very likely ascribable to the exposure of the sample to air. A third minor component is located at 163.7 eV and is compatible with the C−S/C−S−S region, confirming the above-mentioned hypothesis of sulfur interacting with the carbonaceous components of FeBZIM (Figure S12a). Regarding the sulfate sample, the impact of the anion over the surface chemistry of the electrocatalyst is minimal, as shown in the electrochemical section, and is predominantly due to physisorption effects. The lower quality of the spectrum correlates with the lower interaction and hence lower sulfur content compared to sulfide (Table S4). The two major contributions identified in the sulfide sample are now comparable, with an absolute maximum of S^{2-}/Fe−S_2 and a relative maximum of the SO_4^{2-} component. Sulfite is also present, differently than sulfide-contaminated FeBZIM, indicative of a generally higher oxidation degree of the sample. No component in the C−S/C−S−S region was identified (Figure S12b).

From the XPS analysis as a whole, the sulfate contamination of the PGM-free electrocatalyst is not relevant in terms of surface chemistry modification of the electrocatalyst, with a negligible effect over the active sites, hence matching with the electrochemical section. On the contrary, sulfide ions can interact with both Fe-containing active sites and carbonaceous support. The iron contamination most probably occurs in axial configuration, on top of Fe−N_x,[130] while the support modification is at the expense of pending bonds in local

https://doi.org/10.1021/acscatal.2c05222
ACS Catal. 2023, 13, 2162−2175

disruption of the sp^2 C structure. A probable concurring effect is also present at the expense of pyridinic nitrogen. Considering the difference in electronegativity between C and N, and the lone pair located on N, C−N bonds have delocalized charge density allowing a partial positive charge on C and a partial negative charge on N ($C^{\delta+}-N^{\delta-}$), often suggested as C−N active sites for the ORR.[44,131,132] A plausible hypothesis is the preferential interaction of S^{2-} with the positively charged C, corroborated by the increase in the sp^3 region of the C 1s spectrum of sulfide, eventually replacing the N species.

4. OVERALL CONSIDERATIONS AND DISCUSSION

Observing the reported data as a whole, the trends of the electrochemical parameters can be considered peculiar to the different natures of the two electrocatalysts. Pt40CB is a metallic nanoparticle-based material dispersed over a C sp^2 support acting as a dual component structure. FeBZIM and PGM-free electrocatalysts are composed of atomic metal-containing (single metal atom) and metal-free sites (nitrogen functionalities) embedded into the C sp^2 matrix, which directly impacts the catalytic activity. Pt40CB is exceptionally sensitive to sulfide species, with catalytic properties deteriorating rapidly at any pH in the first two steps of concentrations (0.05 and 0.1 mM, see also Figures S9a and S10a) and saturating for the remaining steps. However, the contamination of Pt40CB is reversible to a great extent for all pH values, indicative of the metallic nature of the material, possessing ductility behavior. FeBZIM, on the contrary, can be considered a tenacious material, being poisoned only by the aggressive compound H_2S (pH 1), and the total decrease in performance is comparable to the first step of Pt40CB. However, the recovery in electrocatalytic activity is practically null. Since the difference in active sites between them is trivial, with Pt possessing a vast amount of only one kind of site, PGM-free electrocatalysts can withstand contamination due to the presence of active sites of different natures. Eventually, the effect of chemisorbed S anions could be either a complete deactivation of the metal-containing sites (hence secondary sites are the only ones not affected) or partial deactivation of the sites. For Pt40CB, 0.1 mM H_2S can be considered the point of complete saturation and deactivation of the electrocatalyst, while FeBZIM can withstand 500 times more.

Sulfate poisoning is not associated with chemisorption; hence the impact on the electrocatalysis is negligible and could be ascribable to physisorption effects, whose trends are reported in Figures S6−S8.

Focusing on the acidic environment, the most interesting condition for obvious technological considerations and the only one impacting FeBZIM performance, the consequences of sulfide on Pt surfaces at a pH where the ORR mechanism is strictly surface dependent can be explained using the literature. In this case, the fingerprint of H_2S contamination is associated with a change in the Tafel slope for both HPR and LPR regions of Pt40CB converging toward the value of 120 mV dec^{-1}, typical of simple electron transfer according to the Marcus theory. At low overpotential (HPR zone), the HPR slope increased toward 120 mV dec^{-1} with two steps (0.05 and 0.1 mM) stabilizing afterward. At the same time, at high overpotential (LPR zone), the LPR slope increased first to 180 mV dec^{-1} and then decreased back to the 120 mV dec^{-1} value (Figure S4a,b).

Meanwhile, J_0 from HPR increased rapidly in the same two steps but then leveled to a value (around 8×10^{-7} mA cm^{-2}) higher than the starting point (about 1×10^{-7} mA cm^{-2}). Conversely, J_0 from LPR decreased gradually from $\sim 10^{-3}$ mA cm^{-2} down to $\sim 10^{-6}$ mA cm^{-2}, not far from the stabilized value of the HPR counterpart (to better visualize the trends, please see Figure 2a,b). Ultimately, due to different regions of overpotential, the two components of the ORR are leveled, indicative of a situation where just one phenomenon seems to be occurring. The trend reported for the HPR Tafel slope of Pt40CB is indeed in agreement with the literature,[80] where the increase in the range 0.8−0.9 V from the 60 mV dec^{-1} to higher values was associated with the oxidation of sulfur to sulfates taking place in parallel with/over the oxygen reduction. The event is thus either an S-involving reaction or the $2e^-$ ORR path due to the complete deactivation of Pt and the residual effect of the support, as reported in the literature[94] and matching with the residual activity observed in the LSV.

When FeBZIM is contaminated at pH 1, H_2S gradually impacts the ORR at increased concentration. The HPR slope increased toward the value of 100 mV dec^{-1}. In contrast, J_0(HPR) increased by about one order of magnitude, indicating a more facile reaction associated with the chemisorption phenomenon and occurring in parallel with the ORR, as seen from the increased number of transferred electrons (Figure S5). Similar behavior was observed for nitrite contamination at pH 7,[95] leading to the chemisorption of the nitrosyl ligand.[96,114] However, during S poisoning, the LPR slope also increased but diverged from the value of interest and toward 240 mV dec^{-1}. More importantly, J_0(LPR) maintained almost a stable value (around 10^{-3} mA cm^{-2}) with just a slight increase (above 1 mM) throughout the test (see Figure 2c,d). The reported trend differentiates from both Pt40CB (drastic decrease) and nitrite cases.

Regarding J_0(LPR) of nitrite contamination at pH 7, which was not assessed in our previous paper but is instead reported herein in the Supporting Information, the value in the whole concentration range increased of the same order of magnitude as J_0(HPR), as can be seen in Figure S13. Eventually, the selective impact over the Fe−N_x coordination is translated to the LPR region where secondary sites are untouched (but functioning due to the lower potential). So far, the slight increase of J_0(LPR) of FeBZIM observed is hard to justify.

However, from XPS analysis, the poisoning was found to be a chemisorption effect impacting the surface chemistry of FeBZIM on both the metal-containing sites and the metal-free moieties, with direct contamination of the support, but most important affecting the nitrogen content of the material, especially the pyridinic-N content. According to the literature,[133] the ORR on the PGM-free electrocatalyst at high overpotential (herein LPR zone) has a proton-limited RDS mechanism correlated with peroxide increase. On the contrary, at low overpotential (herein HPR zone), the reaction is proton-independent, and the limitations occurring as onset losses can be ascribed to unspecified aspects.[133] Hence, due to the reported peroxide increase at high overpotential, where the electrocatalyst should operate better since the higher polarization, secondary NC sites must be predominantly responsible for the ORR, known to operate with the $2e^-$ path to peroxide.[134]

Now, the low overpotential region (HPR zone) is easily associable with the Fe−N_x contribution to the ORR through the Fe(III)/Fe(II) redox couple.[35,36] Thus, J_0(HPR) variations

https://doi.org/10.1021/acscatal.2c05222
ACS Catal. 2023, 13, 2162−2175

throughout the contamination test could be ascribable to the modifications of the Fe−N_x sites. Hence, the increase in J_0(HPR) is a marker of a chemisorption effect with secondary reactions over Fe−N_x, as already reported in the nitrite case. Similarly, considering the additional effects of sulfide on support observed with the XPS analysis, the high overpotential ranging from about the half-wave potential to the mass-transport-limited region of LSV (LPR region), and considering the assertion on RDS from the cited literature, it is possible to associate the variation of J_0(LPR) as the descriptor of the Fe−N_x + NC sites upon chemisorption contamination.

The behavior observed for J_0(LPR) of FeBZIM can thus be explained using the H_2S poisoning of Pt and its trends as a reference, as done before with nitrite. Upon contamination of Pt with the S-containing molecule, the ORR electrocatalytic activity decreased drastically. The residual activity recorded, due to the very low potentials required to start, can be associated predominantly with the effect of the support, hence the $2e^-$ reaction observed in the literature.[94,134] We can thus infer that the trend observed for J_0(LPR) of Pt40CB, decreasing drastically and leveling with the J_0(HPR), is the result of the deactivation of primary metallic sites, and the residual catalytic activity is the effect of (eventually contaminated) support, due to the high overpotential applied to operate. Thus, at an increasing contaminant concentration, the impact on the J_0(LPR) of Pt40CB is associated with the remaining support contribution, running with a less efficient ORR, and correlated to a decrease in the exchange current density. Similarly, considering the interconnected nature of the support with primary and secondary sites in PGM-free electrocatalysts, the increase in J_0(HPR) associated with the formation of an electrochemically active adduct over the primary sites of FeBZIM is transposed to the LPR region, summing its contribution with the contribution of the support and secondary sites to the ORR.

Eventually, the difference in the J_0(LPR) of FeBZIM with respect to the nitrite case (considered selective of the Fe−N_x sites) and Pt is ascribable to a combination of concurring phenomena occurring both on Fe−N_x and secondary NC sites together, ending with a J_0(LPR) combination of an increase and a decrease in J_0, respectively, for the former and the latter sites upon contamination. The variation of the J_0(LPR) can thus be correlated to the effect of contamination over Fe−N_x + NC sites as a whole.

5. CONCLUSIONS

Comparing the ORR behavior from acidic to alkaline of Pt/C and PGM-free electrocatalysts resulted in well-known differences in catalytic activity, with Pt/C being more active in acidic pH in terms of onset and half-wave potentials. To match the performance of PGM-free electrocatalysts with Pt/C electrocatalysts, specific protocols have been developed and reported in the literature to evaluate the site density (SD) of the materials and calculate the turnover frequency (TOF). However, to the state of the art, no direct control over the nature of the counted sites was possible by exploiting probing molecules dissolved in the electrolyte solution. In this work, the ORR activity of Pt/C and PGM-free electrocatalysts was tested at pH 1, using H_2S as a poisoning agent in concentrations from 0.05 to 50 mM. The electrochemical measurements carried out on PGM-free electrocatalysts highlighted the changes in the ORR electrocatalytic activity due to sulfide poisoning, and the XPS analysis revealed that sulfide species interact with both metal-containing sites and carbon support, resulting in a decrease in the pyridinic-N content. When primary (Fe-containing) sites are contaminated, the ORR activity decreases. Still, the electron exchange ability of the system increases after contamination, as indicated by the increase of the transferred electrons number and the exchange current density obtained from the first Tafel slope in the high potential region, named J_0(HPR), arising from secondary reactions of the adduct. This finding was actually recurrent as per the nitrite contamination of primary metal-containing sites. Hence, an increase in J_0(HPR) with the contaminant's concentration indicates chemisorption onto Fe−N_x sites. In addition, the trend of J_0(LPR) (low potential region) upon contamination resulted as a combination of two concurring phenomena leading to an increase correlated to chemisorption onto primary sites and a decrease correlated to the impact on support and secondary metal-free sites. Hence, an increase in J_0(LPR) can be associated with the poisoning of both Fe−N_x + NC sites.

Based on these results, it was possible to identify J_0 as a new descriptor capable of discriminating what type of active sites (primary and/or secondary sites) are poisoned in PGM-free electrocatalysts by chemisorption effects. The descriptors proposed can be considered a supporting tool to assist the selection of the probing molecules for further studies of site density evaluation.

■ ASSOCIATED CONTENT

Supporting Information

The Supporting Information is available free of charge at https://pubs.acs.org/doi/10.1021/acscatal.2c05222.

Additional tables and figures regarding LSV-RDE characterization of FeBZIM and Pt40CB at pH 7 and 13; XPS high-resolution N 1s and S 2p spectra of sulfide- and sulfate-contaminated FeBZIM; and explanation of the protocols used for the evaluation of electrochemical parameters used in the main paper (PDF)

■ AUTHOR INFORMATION

Corresponding Authors

Carlo Santoro − *Electrocatalysis and Bioelectrocatalysis Laboratory (EBLab), Department of Material Science, University of Milan Bicocca, 20125 Milan, Italy;* orcid.org/0000-0002-0944-4500; Email: carlo.santoro@unimib.it

Barbara Mecheri − *Department of Chemical Science and Technologies, University of Rome Tor Vergata, 00133 Rome, Italy;* orcid.org/0000-0002-1458-6239; Email: barbara.mecheri@uniroma2.it

Authors

Valerio C. A. Ficca − *Department of Chemical Science and Technologies, University of Rome Tor Vergata, 00133 Rome, Italy; Department of Physics, Sapienza University of Rome, 00185 Roma, Italy*

Ernesto Placidi − *Department of Physics, Sapienza University of Rome, 00185 Roma, Italy;* orcid.org/0000-0002-3820-8451

Fabrizio Arciprete − *Department of Physics, University of Rome Tor Vergata, 00133 Rome, Italy;* orcid.org/0000-0003-3602-3717

https://doi.org/10.1021/acscatal.2c05222
ACS Catal. 2023, 13, 2162−2175

Alexey Serov − *Electrification and Energy Infrastructures Division, Oak Ridge National Laboratory, Oak Ridge, Tennessee 37831, United States*

Plamen Atanassov − *Chemical and Biomolecular Engineering, National Fuel Cell Research Center, University of California, Irvine, Irvine, California 92697, United States;* orcid.org/0000-0003-2996-472X

Complete contact information is available at: https://pubs.acs.org/10.1021/acscatal.2c05222

Author Contributions

This manuscript was written through contributions of all authors. All authors have given approval to the final version of the manuscript.

Notes

The authors declare no competing financial interest.

■ ACKNOWLEDGMENTS

C.S. is funded by the Italian Ministry of Universities and Research (Ministero dell'Università e della Ricerca—MUR) through the "Rita Levi Montalcini 2018" fellowship (Grant number PGR18MAZLI).

■ REFERENCES

(1) Ramaswamy, N.; Tylus, U.; Jia, Q.; Mukerjee, S. Activity Descriptor Identification for Oxygen Reduction on Nonprecious Electrocatalysts: Linking Surface Science to Coordination Chemistry. *J. Am. Chem. Soc.* **2013**, *135*, 15443−15449.

(2) Balali, Y.; Stegen, S. Review of energy storage systems for vehicles based on technology, environmental impacts, and costs. *Renewable Sustainable Energy Rev.* **2021**, *135*, No. 110185.

(3) Kakoulaki, G.; Kougias, I.; Taylor, N.; Dolci, F.; Moya, J.; Jäger-Waldau, A. Green hydrogen in Europe − A regional assessment: Substituting existing production with electrolysis powered by renewables. *Energy Convers. Manage.* **2021**, *228*, No. 113649.

(4) Ramaswamy, N.; Mukerjee, S. Fundamental Mechanistic Understanding of Electrocatalysis of Oxygen Reduction on Pt and Non-Pt Surfaces: Acid versus Alkaline Media. *Adv. Phys. Chem.* **2012**, *2012*, 1−17.

(5) Ramaswamy, N.; Mukerjee, S. Influence of Inner- and Outer-Sphere Electron Transfer Mechanisms during Electrocatalysis of Oxygen Reduction in Alkaline Media. *J. Phys. Chem. C* **2011**, *115*, 18015−18026.

(6) Gasteiger, H. A.; Marković, N. M. Just a Dream—or Future Reality? *Science* **2009**, *324*, 48−49.

(7) Shao, M. Palladium-based electrocatalysts for hydrogen oxidation and oxygen reduction reactions. *J. Power Sources* **2011**, *196*, 2433−2444.

(8) Greeley, J.; Stephens, I. E. L.; Bondarenko, A. S.; Johansson, T. P.; Hansen, H. A.; Jaramillo, T. F.; Rossmeisl, J.; Chorkendorff, I.; Nørskov, J. K. Alloys of platinum and early transition metals as oxygen reduction electrocatalysts. *Nat. Chem.* **2009**, *1*, 552−556.

(9) Lima, F. H. B.; Zhang, J.; Shao, M. H.; Sasaki, K.; Vukmirovic, M. B.; Ticianelli, E. A.; Adzic, R. R. Catalytic Activity−d-Band Center Correlation for the O2 Reduction Reaction on Platinum in Alkaline Solutions. *J. Phys. Chem. C* **2007**, *111*, 404−410.

(10) Gasteiger, H. A.; Kocha, S. S.; Sompalli, B.; Wagner, F. T. Activity benchmarks and requirements for Pt, Pt-alloy, and non-Pt oxygen reduction catalysts for PEMFCs. *Appl. Catal., B* **2005**, *56*, 9−35.

(11) Zagal, J. H.; Specchia, S.; Atanassov, P. Mapping transition metal-MN4 macrocyclic complex catalysts performance for the critical reactivity descriptors. *Curr. Opin. Electrochem.* **2021**, *27*, No. 100683.

(12) Specchia, S.; Atanassov, P.; Zagal, J. H. Mapping transition metal−nitrogen−carbon catalyst performance on the critical descriptor diagram. *Curr. Opin. Electrochem.* **2021**, *27*, No. 100687.

(13) Primbs, M.; Sun, Y.; Roy, A.; Malko, D.; Mehmood, A.; Sougrati, M.-T.; Blanchard, P.-Y.; Granozzi, G.; Kosmala, T.; Daniel, G.; Atanassov, P.; Sharman, J.; Durante, C.; Kucernak, A.; Jones, D.; Jaouen, F.; Strasser, P. Establishing reactivity descriptors for platinum group metal (PGM)-free Fe−N−C catalysts for PEM fuel cells. *Energy Environ. Sci.* **2020**, *13*, 2480−2500.

(14) Luo, F.; Choi, C. H.; Primbs, M. J. M.; Ju, W.; Li, S.; Leonard, N. D.; Thomas, A.; Jaouen, F.; Strasser, P. Accurate Evaluation of Active-Site Density (SD) and Turnover Frequency (TOF) of PGM-Free Metal−Nitrogen-Doped Carbon (MNC) Electrocatalysts using CO Cryo Adsorption. *ACS Catal.* **2019**, *9*, 4841−4852.

(15) Mehmood, A.; Ali, B.; Gong, M.; Gyu Kim, M.; Kim, J.-Y.; Bae, J.-H.; Kucernak, A.; Kang, Y.-M.; Nam, K.-W. Development of a highly active FeNC catalyst with the preferential formation of atomic iron sites for oxygen reduction in alkaline and acidic electrolytes. *J. Colloid Interface Sci.* **2021**, *596*, 148−157.

(16) Jeong, E.-S.; Park, C.-I.; Jin, Z.; Hwang, I.-H.; Son, J.-K.; Kim, M.-Y.; Choi, J.-S.; Han, S.-W. Temperature-Dependent Local Structural Properties of Redox Pt Nanoparticles on TiO2 and ZrO2 Supports. *Catal. Lett.* **2015**, *145*, 971−983.

(17) Verga, L. G.; Aarons, J.; Sarwar, M.; Thompsett, D.; Russell, A. E.; Skylaris, C.-K. Effect of graphene support on large Pt nanoparticles. *Phys. Chem. Chem. Phys.* **2016**, *18*, 32713−32722.

(18) Kattel, S.; Atanassov, P.; Kiefer, B. A density functional theory study of oxygen reduction reaction on non-PGM Fe−Nx−C electrocatalysts. *Phys. Chem. Chem. Phys.* **2014**, *16*, 13800−13806.

(19) Viswanathan, V.; Wang, F. Y.-F. Theoretical analysis of the effect of particle size and support on the kinetics of oxygen reduction reaction on platinum nanoparticles. *Nanoscale* **2012**, *4*, 5110−5117.

(20) Rizo, R.; Herrero, E.; Feliu, J. M. Oxygen reduction reaction on stepped platinum surfaces in alkaline media. *Phys. Chem. Chem. Phys.* **2013**, *15*, 15416−15425.

(21) Wang, X.; Li, Z.; Qu, Y.; Yuan, T.; Wang, W.; Wu, Y.; Li, Y. Review of Metal Catalysts for Oxygen Reduction Reaction: From Nanoscale Engineering to Atomic Design. *Chem* **2019**, *5*, 1486−1511.

(22) Asset, T.; Atanassov, P. Iron-Nitrogen-Carbon Catalysts for Proton Exchange Membrane Fuel Cells. *Joule* **2020**, *4*, 33−44.

(23) Luo, F.; Roy, A.; Silvioli, L.; Cullen, D. A.; Zitolo, A.; Sougrati, M. T.; Oguz, I. C.; Mineva, T.; Teschner, D.; Wagner, S.; Wen, J.; Dionigi, F.; Kramm, U. I.; Rossmeisl, J.; Jaouen, F.; Strasser, P. P-block single-metal-site tin/nitrogen-doped carbon fuel cell cathode catalyst for oxygen reduction reaction. *Nat. Mater.* **2020**, *19*, 1215−1223.

(24) da S Freitas, W.; D'Epifanio, A.; Ficca, V. C. A.; Placidi, E.; Arciprete, F.; Mecheri, B. Tailoring active sites of iron-nitrogen-carbon catalysts for oxygen reduction in alkaline environment: Effect of nitrogen-based organic precursor and pyrolysis atmosphere. *Electrochim. Acta* **2021**, *391*, No. 138899.

(25) da Silva Freitas, W.; Mecheri, B.; Lo Vecchio, C.; Gatto, I.; Baglio, V.; Ficca, V. C. A.; Patra, A.; Placidi, E.; D'Epifanio, A. Metal-organic-framework-derived electrocatalysts for alkaline polymer electrolyte fuel cells. *J. Power Sources* **2022**, *550*, No. 232135.

(26) de Oliveira, M. A. C.; Ficca, V. C. A.; Gokhale, R.; Santoro, C.; Mecheri, B.; D'Epifanio, A.; Licoccia, S.; Atanassov, P. Iron(II) phthalocyanine (FePc) over carbon support for oxygen reduction reaction electrocatalysts operating in alkaline electrolyte. *J. Solid State Electrochem.* **2021**, *25*, 93−104.

(27) Kumar, R.; Sahoo, S.; Joanni, E.; Singh, R. K.; Maegawa, K.; Tan, W. K.; Kawamura, G.; Kar, K. K.; Matsuda, A. Heteroatom doped graphene engineering for energy storage and conversion. *Mater. Today* **2020**, *39*, 47−65.

(28) Yano, H.; Higuchi, E.; Uchida, H.; Watanabe, M. Temperature Dependence of Oxygen Reduction Activity at Nafion-Coated Bulk Pt and Pt/Carbon Black Catalysts. *J. Phys. Chem. B* **2006**, *110*, 16544−16549.

(29) Arruda, T. M.; Shyam, B.; Ziegelbauer, J. M.; Mukerjee, S.; Ramaker, D. E. Investigation into the Competitive and Site-Specific Nature of Anion Adsorption on Pt Using In Situ X-ray Absorption Spectroscopy. *J. Phys. Chem. C* **2008**, *112*, 18087−18097.

(30) Teliska, M.; Murthi, V. S.; Mukerjee, S.; Ramaker, D. E. Correlation of Water Activation, Surface Properties, and Oxygen Reduction Reactivity of Supported Pt−M/C Bimetallic Electrocatalysts Using XAS. *J. Electrochem. Soc.* **2005**, *152*, A2159.
(31) Teliska, M.; O'Grady, W. E.; Ramaker, D. E. Determination of O and OH Adsorption Sites and Coverage in Situ on Pt Electrodes from Pt L23 X-ray Absorption Spectroscopy. *J. Phys. Chem. B* **2005**, *109*, 8076−8084.
(32) Chakraborty, A.; Devivaraprasad, R.; Bera, B.; Neergat, M. Electrochemical estimation of the active site density on metal-free nitrogen-doped carbon using catechol as an adsorbate. *Phys. Chem. Chem. Phys.* **2017**, *19*, 25414−25422.
(33) Rao, C. V.; Cabrera, C. R.; Ishikawa, Y. In Search of the Active Site in Nitrogen-Doped Carbon Nanotube Electrodes for the Oxygen Reduction Reaction. *J. Phys. Chem. Lett.* **2010**, *1*, 2622−2627.
(34) Yasuda, S.; Yu, L.; Kim, J.; Murakoshi, K. Selective nitrogen doping in graphene for oxygen reduction reactions. *Chem. Commun.* **2013**, *49*, 9627−9629.
(35) Tylus, U.; Jia, Q.; Strickland, K.; Ramaswamy, N.; Serov, A.; Atanassov, P.; Mukerjee, S. Elucidating Oxygen Reduction Active Sites in Pyrolyzed Metal−Nitrogen Coordinated Non-Precious-Metal Electrocatalyst Systems. *J. Phys. Chem. C* **2014**, *118*, 8999−9008.
(36) Tylus, U.; Jia, Q.; Hafiz, H.; Allen, R. J.; Barbiellini, B.; Bansil, A.; Mukerjee, S. Engendering anion immunity in oxygen consuming cathodes based on Fe-Nx electrocatalysts: Spectroscopic and electrochemical advanced characterizations. *Appl. Catal., B* **2016**, *198*, 318−324.
(37) Jia, Q.; Ramaswamy, N.; Hafiz, H.; Tylus, U.; Strickland, K.; Wu, G.; Barbiellini, B.; Bansil, A.; Holby, E. F.; Zelenay, P.; Mukerjee, S. Experimental Observation of Redox-Induced Fe−N Switching Behavior as a Determinant Role for Oxygen Reduction Activity. *ACS Nano* **2015**, *9*, 12496−12505.
(38) Mun, Y.; Lee, S.; Kim, K.; Kim, S.; Lee, S.; Han, J. W.; Lee, J. Versatile Strategy for Tuning ORR Activity of a Single Fe-N4 Site by Controlling Electron-Withdrawing/Donating Properties of a Carbon Plane. *J. Am. Chem. Soc.* **2019**, *141*, 6254−6262.
(39) Jaouen, F.; Charreteur, F.; Dodelet, J. P. Fe-Based Catalysts for Oxygen Reduction in PEMFCs: Importance of the Disordered Phase of the Carbon Support. *J. Electrochem. Soc.* **2006**, *153*, A689.
(40) Kanbara, T.; Miyazaki, Y.; Yamamoto, T. New π-conjugated heteroaromatic alternative copolymers with electron-donating thiophene or furan units and electron-withdrawing quinoxaline units: Preparation by palladium-catalyzed polycondensation and characterization of the copolymers. *J. Polym. Sci., Part A: Polym. Chem.* **1995**, *33*, 999−1003.
(41) Cui, Y.; Zhang, X.; Jenekhe, S. A. Thiophene-Linked Polyphenylquinoxaline: A New Electron Transport Conjugated Polymer for Electroluminescent Devices. *Macromolecules* **1999**, *32*, 3824−3826.
(42) Giordano, N.; Antonucci, P. L.; Passalacqua, E.; Pino, L.; Aricò, A. S.; Kinoshita, K. Relationship between physicochemical properties and electrooxidation behaviour of carbon materials. *Electrochim. Acta* **1991**, *36*, 1931−1935.
(43) Boldrin, P.; Malko, D.; Mehmood, A.; Kramm, U. I.; Wagner, S.; Paul, S.; Weidler, N.; Kucernak, A. Deactivation, reactivation and super-activation of Fe-N/C oxygen reduction electrocatalysts: Gas sorption, physical and electrochemical investigation using NO and O2. *Appl. Catal., B* **2021**, *292*, No. 120169.
(44) Artyushkova, K.; Serov, A.; Rojas-Carbonell, S.; Atanassov, P. Chemistry of Multitudinous Active Sites for Oxygen Reduction Reaction in Transition Metal−Nitrogen−Carbon Electrocatalysts. *J. Phys. Chem. C* **2015**, *119*, 25917−25928.
(45) Keith, J. A.; Jerkiewicz, G.; Jacob, T. Theoretical Investigations of the Oxygen Reduction Reaction on Pt(111). *ChemPhysChem* **2010**, *11*, 2779−2794.
(46) Koper, M. T. M. Thermodynamic theory of multi-electron transfer reactions: Implications for electrocatalysis. *J. Electroanal. Chem.* **2011**, *660*, 254−260.
(47) Koper, M. T. M. Theory of multiple proton−electron transfer reactions and its implications for electrocatalysis. *Chem. Sci.* **2013**, *4*, 2710−2723.
(48) Wei, G.-F.; Fang, Y.-H.; Liu, Z.-P. First Principles Tafel Kinetics for Resolving Key Parameters in Optimizing Oxygen Electrocatalytic Reduction Catalyst. *J. Phys. Chem. C* **2012**, *116*, 12696−12705.
(49) Nie, Y.; Li, L.; Wei, Z. Recent advancements in Pt and Pt-free catalysts for oxygen reduction reaction. *Chem. Soc. Rev.* **2015**, *44*, 2168−2201.
(50) Guo, S.; Zhang, S.; Sun, S. Tuning Nanoparticle Catalysis for the Oxygen Reduction Reaction. *Angew. Chem., Int. Ed.* **2013**, *52*, 8526−8544.
(51) Appleby, A. J.Electrocatalysis. In *Comprehensive Treatise of Electrochemistry: Volume 7 Kinetics and Mechanisms of Electrode Processes*; Conway, B. E.; Bockris, J. O.; Yeager, E.; Khan, S. U. M.; White, R. E., Eds.; Springer US: Boston, MA, 1983; pp 173−239.
(52) Murthi, V. S.; Urian, R. C.; Mukerjee, S. Oxygen Reduction Kinetics in Low and Medium Temperature Acid Environment: Correlation of Water Activation and Surface Properties in Supported Pt and Pt Alloy Electrocatalysts. *J. Phys. Chem. B* **2004**, *108*, 11011−11023.
(53) Sgarbi, R.; Kumar, K.; Jaouen, F.; Zitolo, A.; Ticianelli, E. A.; Maillard, F. Oxygen reduction reaction mechanism and kinetics on M-NxCy and M@N-C active sites present in model M-N-C catalysts under alkaline and acidic conditions. *J. Solid State Electrochem.* **2021**, *25*, 45−56.
(54) Rojas-Carbonell, S.; Artyushkova, K.; Serov, A.; Santoro, C.; Matanovic, I.; Atanassov, P. Effect of pH on the Activity of Platinum Group Metal-Free Catalysts in Oxygen Reduction Reaction. *ACS Catal.* **2018**, *8*, 3041−3053.
(55) Malko, D.; Kucernak, A. Kinetic isotope effect in the oxygen reduction reaction (ORR) over Fe-N/C catalysts under acidic and alkaline conditions. *Electrochem. Commun.* **2017**, *83*, 67−71.
(56) Zúñiga, C.; Candia-Onfray, C.; Venegas, R.; Muñoz, K.; Urra, J.; Sánchez-Arenillas, M.; Marco, J. F.; Zagal, J. H.; Recio, F. J. Elucidating the mechanism of the oxygen reduction reaction for pyrolyzed Fe-N-C catalysts in basic media. *Electrochem. Commun.* **2019**, *102*, 78−82.
(57) Meier, J. C.; Galeano, C.; Katsounaros, I.; Topalov, A. A.; Kostka, A.; Schüth, F.; Mayrhofer, K. J. J. Degradation Mechanisms of Pt/C Fuel Cell Catalysts under Simulated Start−Stop Conditions. *ACS Catal.* **2012**, *2*, 832−843.
(58) Sethuraman, V. A.; Weidner, J. W. Analysis of sulfur poisoning on a PEM fuel cell electrode. *Electrochim. Acta* **2010**, *55*, 5683−5694.
(59) Chin, D.-T.; Howard, P. D. Hydrogen Sulfide Poisoning of Platinum Anode in Phosphoric Acid Fuel Cell Electrolyte. *J. Electrochem. Soc.* **1986**, *133*, 2447.
(60) Rodriguez, J. A.; Hrbek, J. Interaction of Sulfur with Well-Defined Metal and Oxide Surfaces: Unraveling the Mysteries behind Catalyst Poisoning and Desulfurization. *Acc. Chem. Res.* **1999**, *32*, 719−728.
(61) Gonzalez-Tejuca, L.; Aika, K.; Namba, S.; Turkevich, J. Poisoning titration technique for determining the number of active centers in a supported platinum catalyst. *J. Phys. Chem. A* **1977**, *81*, 1399−1406.
(62) Somorjai, G. A.On the Mechanism of Sulfur Poisoning of Platinum Catalysts, 1972. https://escholarship.org/uc/item/3km776cj (accessed Jan 14, 2022).
(63) Kumar, K.; Dubau, L.; Mermoux, M.; Li, J.; Zitolo, A.; Nelayah, J.; Jaouen, F.; Maillard, F. On the Influence of Oxygen on the Degradation of Fe-N-C Catalysts. *Angew. Chem.* **2020**, *132*, 3261−3269.
(64) Weiss, J.; Zhang, H.; Zelenay, P. Recent progress in the durability of Fe-N-C oxygen reduction electrocatalysts for polymer electrolyte fuel cells. *J. Electroanal. Chem.* **2020**, *875*, No. 114696.
(65) Santoro, C.; Serov, A.; Stariha, L.; Kodali, M.; Gordon, J.; Babanova, S.; Bretschger, O.; Artyushkova, K.; Atanassov, P. Iron based catalysts from novel low-cost organic precursors for enhanced

https://doi.org/10.1021/acscatal.2c05222
ACS Catal. 2023, 13, 2162−2175

oxygen reduction reaction in neutral media microbial fuel cells. *Energy Environ. Sci.* **2016**, *9*, 2346−2353.
(66) Santoro, C.; Serov, A.; Villarrubia, C. W. N.; Stariha, S.; Babanova, S.; Artyushkova, K.; Schuler, A. J.; Atanassov, P. High catalytic activity and pollutants resistivity using Fe-AAPyr cathode catalyst for microbial fuel cell application. *Sci. Rep.* **2015**, *5*, No. 16596.
(67) Jing, F.; Hou, M.; Shi, W.; Fu, J.; Yu, H.; Ming, P.; Yi, B. The effect of ambient contamination on PEMFC performance. *J. Power Sources* **2007**, *166*, 172−176.
(68) Imamura, D.; Yamaguchi, E. Effect of Air Contaminants on the Electrolyte Degradation in Polymer Electrolyte Membrane Fuel Cells. *ECS Trans.* **2009**, *25*, 813.
(69) Moore, J. M.; Adcock, P. L.; Lakeman, J. B.; Mepsted, G. O. The effects of battlefield contaminants on PEMFC performance. *J. Power Sources* **2000**, *85*, 254−260.
(70) Nasri, N. S.; Jones, J. M.; Dupont, V. A.; Williams, A. A Comparative Study of Sulfur Poisoning and Regeneration of Precious-Metal Catalysts. *Energy Fuels* **1998**, *12*, 1130−1134.
(71) Trens, P.; Durand, R.; Coq, B.; Coutanceau, C.; Rousseau, S.; Lamy, C. Poisoning of Pt/C catalysts by CO and its consequences over the kinetics of hydrogen chemisorption. *Appl. Catal., B* **2009**, *92*, 280−284.
(72) Cheng, X.; Shi, Z.; Glass, N.; Zhang, L.; Zhang, J.; Song, D.; Liu, Z.-S.; Wang, H.; Shen, J. A review of PEM hydrogen fuel cell contamination: Impacts, mechanisms, and mitigation. *J. Power Sources* **2007**, *165*, 739−756.
(73) Nagahara, Y.; Sugawara, S.; Shinohara, K. The impact of air contaminants on PEMFC performance and durability. *J. Power Sources* **2008**, *182*, 422−428.
(74) Garzon, F. H.; Uribe, F. A.Effects of Contaminants on Catalyst Activity. In *Handbook of Fuel Cells—Fundamentals, Technology and Applications, Advances in Electrocatalysis, Materials, Diagnostics and Durability*; Vielstich, W.; Gasteiger, H. A.; Lamm, A.; Yokokawa, H., Eds.; John Wiley & Sons, 2010.
(75) Hongsirikarn, K.; Napapruekchart, T.; Mo, X.; Goodwin, J. G. Effect of ammonium ion distribution on Nafion conductivity. *J. Power Sources* **2011**, *196*, 644−651.
(76) Yuan, X.-Z.; Li, H.; Yu, Y.; Jiang, M.; Qian, W.; Zhang, S.; Wang, H.; Wessel, S.; Cheng, T. T. H. Diagnosis of contamination introduced by ammonia at the cathode in a polymer electrolyte membrane fuel cell. *Int. J. Hydrogen Energy* **2012**, *37*, 12464−12473.
(77) Baturina, O. A.; Swider-Lyons, K. E. Effect of SO2 on the Performance of the Cathode of a PEM Fuel Cell at 0.5−0.7 V. *J. Electrochem. Soc.* **2009**, *156*, No. B1423.
(78) Sharma, H. N.; Sharma, V.; Mhadeshwar, A. B.; Ramprasad, R. Why Pt Survives but Pd Suffers From SOx Poisoning? *J. Phys. Chem. Lett.* **2015**, *6*, 1140−1148.
(79) Tsushima, S.; Kaneko, K.; Morioka, H.; Hirai, S. Influence of SO2 Concentration and Relative Humidity on Electrode Poisoning in Polymer Electrolyte Membrane Fuel Cells. *J. Therm. Sci. Technol.* **2012**, *7*, 619−632.
(80) Gould, B. D.; Baturina, O. A.; Swider-Lyons, K. E. Deactivation of Pt/VC proton exchange membrane fuel cell cathodes by SO2, H2S and COS. *J. Power Sources* **2009**, *188*, 89−95.
(81) Lopes, T.; Chlistunoff, J.; Sansiñena, J.-M.; Garzon, F. H. Oxygen reduction reaction on a Pt/carbon fuel cell catalyst in the presence of trace quantities of ammonium ions: An RRDE study. *Int. J. Hydrogen Energy* **2012**, *37*, 5202−5207.
(82) He, Q.; Shyam, B.; Nishijima, M.; Ramaker, D.; Mukerjee, S. Mitigating Phosphate Anion Poisoning of Cathodic Pt/C Catalysts in Phosphoric Acid Fuel Cells. *J. Phys. Chem. C* **2013**, *117*, 4877−4887.
(83) Yang, D.; Ma, J.; Xu, L.; Wu, M.; Wang, H. The effect of nitrogen oxides in air on the performance of proton exchange membrane fuel cell. *Electrochim. Acta* **2006**, *51*, 4039−4044.
(84) Chen, M.; Du, C.; Zhang, J.; Wang, P.; Zhu, T. Effect, mechanism and recovery of nitrogen oxides poisoning on oxygen reduction reaction at Pt/C catalysts. *J. Power Sources* **2011**, *196*, 620−626.
(85) He, J.; Shen, Y.; Yang, M.; Zhang, H.; Deng, Q.; Ding, Y. The effect of surface strain on the CO-poisoned surface of Pt electrode for hydrogen adsorption. *J. Catal.* **2017**, *350*, 212−217.
(86) Zhu, X.; Cheng, B.; Yu, J.; Ho, W. Halogen poisoning effect of Pt-TiO2 for formaldehyde catalytic oxidation performance at room temperature. *Appl. Surf. Sci.* **2016**, *364*, 808−814.
(87) Marković, N.; Gasteiger, H. A.; Grgur, B. N.; Ross, P. N. Oxygen reduction reaction on Pt(111): effects of bromide. *J. Electroanal. Chem.* **1999**, *467*, 157−163.
(88) Schmidt, T. J.; Paulus, U. A.; Gasteiger, H. A.; Behm, R. J. The oxygen reduction reaction on a Pt/carbon fuel cell catalyst in the presence of chloride anions. *J. Electroanal. Chem.* **2001**, *508*, 41−47.
(89) Stamenkovic, V.; Markovic, N. M.; Ross, P. N. Structure-relationships in electrocatalysis: oxygen reduction and hydrogen oxidation reactions on Pt(111) and Pt(100) in solutions containing chloride ions. *J. Electroanal. Chem.* **2001**, *500*, 44−51.
(90) Song, S. Q.; Zhou, W. J.; Li, W. Z.; Sun, G.; Xin, Q.; Kontou, S.; Tsiakaras, P. Direct methanol fuel cells: Methanol crossover and its influence on single DMFC performance. *Ionics* **2004**, *10*, 458−462.
(91) Imabayashi, S.-i.; Kondo, Y.; Komori, R.; Kawano, A.; Ohsaka, T. Effects of Atmospheric Trace Species on the Oxygen Reduction Reaction and the Production of Hydrogen Peroxide. *ECS Trans.* **2008**, *16*, 925.
(92) Mohtadi, R.; Lee, W.-k.; Van Zee, J. W. Assessing durability of cathodes exposed to common air impurities. *J. Power Sources* **2004**, *138*, 216−225.
(93) Dunleavy, J. Final Analysis. *Platinum Met. Rev.* **2006**, *50*, 110.
(94) Garsany, Y.; Baturina, O. A.; Swider-Lyons, K. E. Impact of Sulfur Dioxide on the Oxygen Reduction Reaction at Pt/Vulcan Carbon Electrocatalysts. *J. Electrochem. Soc.* **2007**, *154*, B670.
(95) Ficca, V. C. A.; Santoro, C.; D'Epifanio, A.; Licoccia, S.; Serov, A.; Atanassov, P.; Mecheri, B. Effect of Active Site Poisoning on Iron−Nitrogen−Carbon Platinum-Group-Metal-Free Oxygen Reduction Reaction Catalysts Operating in Neutral Media: A Rotating Disk Electrode Study. *ChemElectroChem* **2020**, *7*, 3044−3055.
(96) Malko, D.; Kucernak, A.; Lopes, T. In situ electrochemical quantification of active sites in Fe−N/C non-precious metal catalysts. *Nat. Commun.* **2016**, *7*, No. 13285.
(97) Bae, G.; Kim, H.; Choi, H.; Jeong, P.; Kim, D. H.; Kwon, H. C.; Lee, K.-S.; Choi, M.; Oh, H.-S.; Jaouen, F.; Choi, C. H. Quantification of Active Site Density and Turnover Frequency: From Single-Atom Metal to Nanoparticle Electrocatalysts. *JACS Au* **2021**, *1*, 586−597.
(98) Yang, W.; Li, J.; Lan, L.; Fu, Q.; Zhang, L.; Zhu, X.; Liao, Q. Poison tolerance of non-precious catalyst towards oxygen reduction reaction. *Int. J. Hydrogen Energy* **2018**, *43*, 8474−8479.
(99) Birry, L.; Zagal, J. H.; Dodelet, J.-P. Does CO poison Fe-based catalysts for ORR? *Electrochem. Commun.* **2010**, *12*, 628−631.
(100) Reshetenko, T.; Serov, A.; Artyushkova, K.; Matanovic, I.; Stariha, S.; Atanassov, P. Tolerance of non-platinum group metals cathodes proton exchange membrane fuel cells to air contaminants. *J. Power Sources* **2016**, *324*, 556−571.
(101) Sebastián, D.; Serov, A.; Artyushkova, K.; Atanassov, P.; Aricò, A. S.; Baglio, V. Performance, methanol tolerance and stability of Fe-aminobenzimidazole derived catalyst for direct methanol fuel cells. *J. Power Sources* **2016**, *319*, 235−246.
(102) Malko, D.; Lopes, T.; Symianakis, E.; Kucernak, A. R. The intriguing poison tolerance of non-precious metal oxygen reduction reaction (ORR) catalysts. *J. Mater. Chem. A* **2016**, *4*, 142−152.
(103) Thorum, M. S.; Hankett, J. M.; Gewirth, A. A. Poisoning the Oxygen Reduction Reaction on Carbon-Supported Fe and Cu Electrocatalysts: Evidence for Metal-Centered Activity. *J. Phys. Chem. Lett.* **2011**, *2*, 295−298.
(104) von Deak, D.; Singh, D.; Biddinger, E. J.; King, J. C.; Bayram, B.; Miller, J. T.; Ozkan, U. S. Investigation of sulfur poisoning of CNx oxygen reduction catalysts for PEM fuel cells. *J. Catal.* **2012**, *285*, 145−151.
(105) von Deak, D.; Singh, D.; King, J. C.; Ozkan, U. S. Use of carbon monoxide and cyanide to probe the active sites on nitrogen-

https://doi.org/10.1021/acscatal.2c05222
ACS Catal. 2023, 13, 2162−2175

doped carbon catalysts for oxygen reduction. *Appl. Catal., B* **2012**, *113*−*114*, 126−133.
(106) Mamtani, K.; Jain, D.; Zemlyanov, D.; Celik, G.; Luthman, J.; Renkes, G.; Co, A. C.; Ozkan, U. S. Probing the Oxygen Reduction Reaction Active Sites over Nitrogen-Doped Carbon Nanostructures (CNx) in Acidic Media Using Phosphate Anion. *ACS Catal.* **2016**, *6*, 7249−7259.
(107) Chung, M. W.; Chon, G.; Kim, H.; Jaouen, F.; Choi, C. H. Electrochemical Evidence for Two Sub-families of FeNxCy Moieties with Concentration-Dependent Cyanide Poisoning. *ChemElectroChem* **2018**, *5*, 1880−1885.
(108) Chen, Y.; Artyushkova, K.; Rojas-Carbonell, S.; Serov, A.; Matanovic, I.; Santoro, C.; Asset, T.; Atanassov, P. Inhibition of Surface Chemical Moieties by Tris(hydroxymethyl)aminomethane: A Key to Understanding Oxygen Reduction on Iron−Nitrogen−Carbon Catalysts. *ACS Appl. Energy Mater.* **2018**, *1*, 1942−1949.
(109) Yang, X.; Xia, D.; Kang, Y.; Du, H.; Kang, F.; Gan, L.; Li, J. Unveiling the Axial Hydroxyl Ligand on Fe-N4-C Electrocatalysts and Its Impact on the pH-Dependent Oxygen Reduction Activities and Poisoning Kinetics. *Adv. Sci.* **2020**, *7*, No. 2000176.
(110) Jiang, W.-J.; Gu, L.; Li, L.; Zhang, Y.; Zhang, X.; Zhang, L.-J.; Wang, J.-Q.; Hu, J.-S.; Wei, Z.; Wan, L.-J. Understanding the High Activity of Fe−N−C Electrocatalysts in Oxygen Reduction: Fe/Fe3C Nanoparticles Boost the Activity of Fe−Nx. *J. Am. Chem. Soc.* **2016**, *138*, 3570−3578.
(111) Wei, X.; Luo, X.; Wang, H.; Gu, W.; Cai, W.; Lin, Y.; Zhu, C. Highly-defective Fe-N-C catalysts towards pH-Universal oxygen reduction reaction. *Appl. Catal., B* **2020**, *263*, No. 118347.
(112) Wang, Q.; Zhou, Z.-Y.; Lai, Y.-J.; You, Y.; Liu, J.-G.; Wu, X.-L.; Terefe, E.; Chen, C.; Song, L.; Rauf, M.; Tian, N.; Sun, S.-G. Phenylenediamine-Based FeNx/C Catalyst with High Activity for Oxygen Reduction in Acid Medium and Its Active-Site Probing. *J. Am. Chem. Soc.* **2014**, *136*, 10882−10885.
(113) Singh, D.; Mamtani, K.; Bruening, C. R.; Miller, J. T.; Ozkan, U. S. Use of H2S to Probe the Active Sites in FeNC Catalysts for the Oxygen Reduction Reaction (ORR) in Acidic Media. *ACS Catal.* **2014**, *4*, 3454−3462.
(114) Malko, D.; Kucernak, A.; Lopes, T. Performance of Fe−N/C Oxygen Reduction Electrocatalysts toward NO2−, NO, and NH2OH Electroreduction: From Fundamental Insights into the Active Center to a New Method for Environmental Nitrite Destruction. *J. Am. Chem. Soc.* **2016**, *138*, 16056−16068.
(115) Li, Y.; Zhou, W.; Wang, H.; Xie, L.; Liang, Y.; Wei, F.; Idrobo, J.-C.; Pennycook, S. J.; Dai, H. An oxygen reduction electrocatalyst based on carbon nanotube−graphene complexes. *Nat. Nanotechnol.* **2012**, *7*, 394−400.
(116) Ficca, V. C. A.; Santoro, C.; Marsili, E.; da Silva Freitas, W.; Serov, A.; Atanassov, P.; Mecheri, B. Sensing nitrite by iron-nitrogen-carbon oxygen reduction electrocatalyst. *Electrochim. Acta* **2022**, *402*, No. 139514.
(117) Mecheri, B.; Gokhale, R.; Santoro, C.; Costa de Oliveira, M. A.; D'Epifanio, A.; Licoccia, S.; Serov, A.; Artyushkova, K.; Atanassov, P. Oxygen Reduction Reaction Electrocatalysts Derived from Iron Salt and Benzimidazole and Aminobenzimidazole Precursors and Their Application in Microbial Fuel Cell Cathodes. *ACS Appl. Energy Mater.* **2018**, *1*, 5755−5765.
(118) Shi, W.; Yi, B.; Hou, M.; Jing, F.; Ming, P. Hydrogen sulfide poisoning and recovery of PEMFC Pt-anodes. *J. Power Sources* **2007**, *165*, 814−818.
(119) Poh, H. L.; Šimek, P.; Sofer, Z.; Pumera, M. Sulfur-Doped Graphene via Thermal Exfoliation of Graphite Oxide in H2S, SO2, or CS2 Gas. *ACS Nano* **2013**, *7*, 5262−5272.
(120) Daniel, G.; Mazzucato, M.; Brandiele, R.; De Lazzari, L.; Badocco, D.; Pastore, P.; Kosmala, T.; Granozzi, G.; Durante, C. Sulfur Doping versus Hierarchical Pore Structure: The Dominating Effect on the Fe−N−C Site Density, Activity, and Selectivity in Oxygen Reduction Reaction Electrocatalysis. *ACS Appl. Mater. Interfaces* **2021**, *13*, 42693−42705.
(121) Descostes, M.; Mercier, F.; Thromat, N.; Beaucaire, C.; Gautier-Soyer, M. Use of XPS in the determination of chemical environment and oxidation state of iron and sulfur samples: constitution of a data basis in binding energies for Fe and S reference compounds and applications to the evidence of surface species of an oxidized pyrite in a carbonate medium. *Appl. Surf. Sci.* **2000**, *165*, 288−302.
(122) Pu, M.; Ma, Y.; Wan, J.; Wang, Y.; Huang, M.; Chen, Y. Fe/S doped granular activated carbon as a highly active heterogeneous persulfate catalyst toward the degradation of Orange G and diethyl phthalate. *J. Colloid Interface Sci.* **2014**, *418*, 330−337.
(123) Volmer-Uebing, M.; Stratmann, M. A surface analytical and an electrochemical study of iron surfaces modified by thiols. *Appl. Surf. Sci.* **1992**, *55*, 19−35.
(124) Biddinger, E. J.; Knapke, D. S.; von Deak, D.; Ozkan, U. S. Effect of sulfur as a growth promoter for CNx nanostructures as PEM and DMFC ORR catalysts. *Appl. Catal., B* **2010**, *96*, 72−82.
(125) Yu, X.-g.; Xie, J.-y.; Yang, J.; Huang, H.-j.; Wang, K.; Wen, Z.-s. Lithium storage in conductive sulfur-containing polymers. *J. Electroanal. Chem.* **2004**, *573*, 121−128.
(126) Contamin, O.; Debiemme-Chouvy, C.; Savy, M.; Scarbeck, G. O2 Electroreduction Catalysis: Effects of Sulfur Addition on Some Cobalt Macrocycles. *J. New Mater. Electrochem. Syst.* **2000**, 67.
(127) Darmstadt, H.; Roy, C. Surface spectroscopic study of basic sites on carbon blacks. *Carbon* **2003**, *41*, 2662−2665.
(128) Bag, S.; Mondal, B.; Das, A. K.; Raj, C. R. Nitrogen and Sulfur Dual-Doped Reduced Graphene Oxide: Synergistic Effect of Dopants Towards Oxygen Reduction Reaction. *Electrochim. Acta* **2015**, *163*, 16−23.
(129) Kiciński, W.; Sęk, J. P.; Matysiak-Brynda, E.; Miecznikowski, K.; Donten, M.; Budner, B.; Nowicka, A. M. Enhancement of PGM-free oxygen reduction electrocatalyst performance for conventional and enzymatic fuel cells: The influence of an external magnetic field. *Appl. Catal., B* **2019**, *258*, No. 117955.
(130) Pavlik, J. W.; Noll, B. C.; Oliver, A. G.; Schulz, C. E.; Scheidt, W. R. Hydrosulfide (HS−) Coordination in Iron Porphyrinates. *Inorg. Chem.* **2010**, *49*, 1017−1026.
(131) Singh, S. K.; Takeyasu, K.; Nakamura, J. Active Sites and Mechanism of Oxygen Reduction Reaction Electrocatalysis on Nitrogen-Doped Carbon Materials. *Adv. Mater.* **2019**, *31*, No. 1804297.
(132) Santoro, C.; Rojas-Carbonell, S.; Awais, R.; Gokhale, R.; Kodali, M.; Serov, A.; Artyushkova, K.; Atanassov, P. Influence of platinum group metal-free catalyst synthesis on microbial fuel cell performance. *J. Power Sources* **2018**, *375*, 11−20.
(133) Chen, Y.; Asset, T.; Lee, R.; Artyushkova, K.; Atanassov, P. Kinetic Isotopic Effect Studies of Iron−Nitrogen−Carbon Electrocatalysts for Oxygen Reduction Reaction. *J. Phys. Chem. C* **2019**, *123*, 11476−11483.
(134) Kinoshita, D. K.*Electrochemical Oxygen Technology*; John Wiley & Sons, 1992; p 448.

https://doi.org/10.1021/acscatal.2c05222
ACS Catal. 2023, 13, 2162−2175